Titre: Title:	Effect of Stereochemistry and Molecular Weight on the Thermal and Rheological Behavior of Poly(L-lactide) and Poly(meso-lactide) Blends
Auteur: Author:	Maude Sicotte-Brisson
Date:	2026
Type:	Mémoire ou thèse / Dissertation or Thesis
Référence: Citation:	Sicotte-Brisson, M. (2026). Effect of Stereochemistry and Molecular Weight on the Thermal and Rheological Behavior of Poly(L-lactide) and Poly(meso-lactide) Blends [Master's thesis, Polytechnique Montréal]. PolyPublie. https://publications.polymtl.ca/76919/

POLYTECHNIQUE MONTRÉAL

affiliée à l'Université de Montréal

Effect of Stereochemistry and Molecular Weight on the Thermal and Rheological Behavior of Poly(L-lactide) and Poly(meso-lactide) Blends

MAUDE SICOTTE-BRISSON

Département de génie chimique

Mémoire présenté en vue de l'obtention du diplôme de *Maîtrise ès sciences appliquées*

Génie chimique

Mai 2026

POLYTECHNIQUE MONTRÉAL

affiliée à l'Université de Montréal

Ce mémoire intitulé :

Effect of Stereochemistry and Molecular Weight on the Thermal and Rheological Behavior of Poly(L-lactide) and Poly(meso-lactide) Blends

présenté par **Maude SICOTTE-BRISSON**

en vue de l'obtention du diplôme de *Maîtrise ès sciences appliquées*

a été dûment accepté par le jury d'examen constitué de :

Charles DUBOIS, président
Marie-Claude HEUZEY, membre et directrice de recherche
Pierre CARREAU, membre et codirecteur de recherche
Marie-Josée DUMONT, membre et codirectrice de recherche
Basil FAVIS, membre

DEDICATION

To my family and Thomas, thank you for all your love and support.

ACKNOWLEDGEMENTS

I would first like to express my sincere gratitude to my research director, Marie-Claude Heuzey, for taking a chance on me and for her constant support, guidance, and encouragement throughout this project.

I would also like to thank my co-directors, Marie-Josée Dumont and Pierre Carreau, for their valuable advice and insightful discussions, which greatly contributed to this work.

I am especially grateful to Patricia Moraille for her tremendous efforts and expertise with the AFM experiments.

I would also like to thank Jed Randall for his helpful discussions and support during the entire course of this project.

RÉSUMÉ

Cette étude examine le comportement thermique, rhéologique et la morphologie du poly(L-lactide) (PLLA), du poly(méso-lactide) et de leurs mélanges sur une large gamme de composition. Les caractérisations ont été réalisées par calorimétrie différentielle à balayage (DSC), microscopie à force atomique (AFM) et rhéométrie. Une miscibilité partielle est suspectée pour les compositions de 10% et 90% w/w% $_{HMW}$PLLA/ $_{HMW}$PMLA, tandis que les compositions de 30 w%, 50 w% et 70 w% de PLLA à faible et haut poids moléculaire semblent plutôt immiscibles. La DSC a révélé des températures de transitions vitreuses (T_g) plus faibles pour le PMLA que pour le PLLA, lesquelles augmentaient avec le poids moléculaire, soit 47.6 ± 0.1 °C pour le $_{LMW}$PMLA et 48.2 ± 0.1 °C pour le $_{HMW}$PMLA, et 61.5 ± 0.1 °C pour le $_{LMW}$PLLA et 61.8 ± 0.4 °C pour le $_{HMW}$PLLA. La DSC a également révélé la présence de deux T_g pour les mélanges supposés immiscibles, correspondant à celles des phases pures, pour l'ensemble des mélanges de PLLA et PMLA à faible et haut poids moléculaire. Enfin, une seule T_g a été observée pour les mélanges partiellement miscibles, soit les mélanges de 10% et 90% w/w% $_{HMW}$PLLA/ $_{HMW}$PMLA. Les observations effectuées via AFM ont révélé une morphologie de type émulsion pour les compositions contenant 30 w% et 70 w% de $_{HMW}$PLLA, et une structure co-continue pour le mélange de 50 w% $_{HMW}$PLLA. L'AFM a aussi relevé la présence de phase mineur dans la phase majeur et vice versa pour les mélanges 30 w% et 70 w% de $_{HMW}$PLLA, indiquant une possible miscibilité partielle ou la simple présence d'hétérogénéité dû à la cristallinité du PLLA pour ces compositions. Les résultats obtenus par cisaillement oscillatoire à faible déformation (SAOS en anglais) ont démontré que le PLLA a une plus haute viscosité que pour le PMLA, et que la viscosité du PLLA et du PMLA augmente avec le poids moléculaire. La règle de Cox Merz a été vérifiée pour le PLLA et le PMLA, et les essais en balayage de temps ont révélé que le PMLA se dégrade plus rapidement et à une température plus faible que le PLLA. Les résutats SAOS ont aussi révélés la présence d'un épaulement à basse fréquence dans le module élastique pour tous les mélanges immiscibles à faible et haut poids moléculaire, ainsi qu'un plus léger épaulement pour les mélanges partiellement miscibles. Les modèles de Palierne et de Gramespacher–Meissner ont permis d'ajuster efficacement les données SAOS des mélanges supposés immiscibles de $_{HMW}$PLLA et de $_{HMW}$PMLA et d'estimer le temps de relaxation de la phase dispersée, renforçant ainsi l'hypothèse d'immiscibilité pour ces compositions. Des diagrammes Cole–Cole et des spectres de relaxation ont été obtenus pour tous les mélanges $_{HMW}$PLLA et $_{HMW}$PMLA, montrant deux modes de

relaxation distincts pour les compositions immiscibles. Ces résultats suggèrent que les mélanges de PMLA et de PLLA sont immiscibles aux compositions intermédiaires, avec une miscibilité partielle à faible et à forte teneur en PLLA, et que les différences stéréochimiques entre le PLLA et le PMLA conduisent à des comportements distincts. Des études complémentaires sur les mécanismes de biodégradation et les propriétés mécaniques de ces matériaux seront nécessaires afin de mieux comprendre le potentiel du PMLA.

ABSTRACT

This study investigates the thermal, rheological behavior, and morphology of poly(L-lactide) (PLLA), poly(meso-lactide) and their blends across a wide composition range. Characterizations were performed using differential scanning calorimetry (DSC), atomic force microscopy (AFM) and rheometry. Partial miscibility is suspected for the 10% and 90% w/w% $_{HMW}$PLLA/ $_{HMW}$PMLA compositions, while 30 w%, 50 w% and 70 w% of low and high molecular weight PLLA compositions exhibited immiscibility. DSC revealed lower glass transitions temperatures (T_g) for PMLA than PLLA that increased with molecular weight, specifically 47.6 ± 0.1 °C for $_{LMW}$PMLA and 48.2 ± 0.1 °C for $_{HMW}$PMLA, and 61.5 ± 0.1 °C for $_{LMW}$PLLA and 61.8 ± 0.4 °C for $_{HMW}$PLLA. DSC also revealed two T_g for immiscible blends, corresponding to those of the neat phases, for all HMW and LMW PLLA and PMLA blends. Finally, a single T_g was observed for partially miscible blends, the blends of 10% and 90% w/w% $_{HMW}$PLLA/ $_{HMW}$PMLA. AFM revealed an emulsion-type morphology at 30 w% and 70 w% $_{HMW}$PLLA compositions, and a co-continuous structure at 50 w% $_{HMW}$PLLA. It also revealed the presence of minor phase in the major phase and vice versa for the blends of 30 w% et 70 w% de $_{HMW}$PLLA, indicating possible partial miscibility or heterogeneity caused by PLLA semi-crystalline nature for these compositions. Small amplitude oscillatory shear (SAOS) results demonstrated that PLLA has a higher viscosity than PMLA, and that the viscosity of PLLA and PMLA increases with molecuar weight. The Cox Merz rule was validated for PLLA and PMLA and time sweep revealed that PMLA degrades at a lower temperature and more rapidly than PLLA. SAOS data also presented a shoulder in the low frequency storage modulus for all immiscible blends of low and high molecular weight, and a slight shoulder for partially miscible blend. The Palierne and the Gramespacher–Meissner models effectively fitted the immiscible compositions SAOS data of $_{HMW}$PLLA and $_{HMW}$PMLA blends and estimated the dispersed phase relaxation time, reinforcing the immiscibility hypothesis. Cole-Cole plot and relaxation spectra were obtained for all $_{HMW}$PLLA and $_{HMW}$PMLA blends, showing distinctly two relaxations modes for immiscible compositions. These results suggest that PMLA and PLLA blends are immiscible at intermediate compositions, with suspected partial miscibility at low and high PLLA content and that the stereochemical differences between PLLA and PMLA lead to distinct behaviors. Complementary investigations into the biodegradation mechanisms and mechanical properties of these materials are needed to better understand the potential of PMLA.

TABLE OF CONTENTS

LIST OF TABLES

LIST OF FIGURES

LIST OF SYMBOLS AND ABBREVIATIONS

ω	Angular Frequency
AFM	Atomic Force Microscopy
T_c	Crystallisation Transition Temperature
T_{cc}	Cold Crystallisation Transition Temperature
η^*	Complex Viscosity
DSC	Differential Scanning Calorimetry
DMA	Dynamic Mechanical Analysis
T_g	Glass Transition Temperature
GM	Gramespacher–Meissner
α	Interfacial Tension
G''	Loss Modulus
LA	Lactic Acid
T_m	Melt Transition Temperature
ML	Mixing Law
G	Modulus
PLA	Polylactic Acid
PLLA	Poly(L-lactide)
PDLA	Poly(D-lactide)
PMLA	Poly(meso-lactide)
PDLLA	Poly(DL-lactide)
R	Radius
$H(\lambda)$	Relaxation Time Spectrum
λ	Relaxation Time

ROP	Ring Opening Polymerization
SAOS	Small Amplitude Oscillatory Shear
G’	Storage Modulus
TGA	Thermogravimetric Analysis
η	Viscosity
κ	Viscosity Ratio
ϕ	Volume Fraction
w	Weight Fraction

LIST OF APPENDICES

CHAPTER 1 INTRODUCTION

1.1 Context

Because of their low production cost, durability, and good mechanical properties, plastics derived from petrochemical resources are omnipresent in modern society. However, in addition to generating significant greenhouse gas emissions during their production phase, they are difficult to manage at the end of their service life. Indeed, only about 9% of plastic waste is recycled worldwide, while the remaining fraction persists in the environment for long periods of time. This persistence contributes to the formation of microplastics, which accumulate in marine ecosystems as well as throughout the food chain. Despite these environmental concerns, plastics remain essential for a wide range of applications. It is therefore crucial to develop more sustainable alternatives [1].

Polylactic acid (PLA) is a bio-based polymer that can be produced from renewable biomass sources such as corn. It is often regarded as one of the most promising alternatives to petrochemical plastics, owing to its favorable mechanical properties, biocompatibility, and potential biodegradability. As a result, PLA has been the subject of extensive research aimed at improving its performance and expanding its range of applications [2]. While conventional PLA, particularly poly(L-lactide) (PLLA), has been extensively studied and is already used in commercial applications, alternative lactic-acid–based polymers are attracting increasing attention due to their enhanced environmental performance. Poly(meso-lactide) (PMLA) has emerged as an interesting candidate, as it promises higher degradability compared to PLLA, making it particularly attractive for applications requiring accelerated end-of-life degradation.

Despite this potential, the fundamental melt rheology of PMLA and its behavior in polymer blends remain largely unexplored. In this context, blending PMLA with PLLA, a well-characterized polymer, provides insight into the impact of PMLA on the melt rheological and thermal behavior of PLLA, as well as the miscibility of the blend under processing conditions.

1.2 Thesis organization

This thesis consists of six chapters. Chapter 2 reviews the existing literature on melt rheology, polylactide (PLA), and the characterization of binary polymer blends. Chapter 3 details the objectives of this research. Chapter 4 presents the results of this work in the form of a scientific article. Chapter 5 reports additional results and Chapter 6 concludes this thesis.

CHAPTER 2 LITTERATURE REVIEW

2.1 Polymer Melt Rheology

Polymers are typically processed in the melt state through operations such as extrusion, injection molding or film blowing. Rheology, the study of the deformation and flow of matter, is essential not only to predict processing behavior but also to understand polymer's behavior on the molecular level.

Polymer melts can be deformed under different flow fields, primarily shear and elongational flows. Shear deformation is most commonly studied due to its relative experimental simplicity and its importance to many industrial processes, such as extrusion and injection molding. In shear flow, adjacent layers of material slide past one another, generating a velocity gradient perpendicular to the flow direction. In contrast, elongational flow involves the stretching or extension of the material along one or more principal axes. Elongational flow is also important in processes such as fiber spinning and film blowing, but is more challenging to characterize experimentally [3].

Several rheological properties are typically used to describe polymer melt behavior during these imposed deformations. One of the key properties under shear deformation includes viscosity (η), which can be described as the resistance of the material to flow. Polymers viscosity is characterized by shear thinning, implying the viscosity decreases with increasing shear rate, unlike a Newtonian fluid, for which viscosity is independent of shear rate. Polymers melts also exhibit viscoelastic behavior, meaning they display both viscous and elastic responses when subjected to deformation. Other important properties include storage and loss moduli. The storage modulus (G'), represents the elastic energy stored during deformation, and the loss modulus (G''), represents the viscous energy dissipated as heat [3].

Small-amplitude oscillatory shear (SAOS) is a common linear viscoelastic experiment, to quantify material relaxation characteristics. In SAOS, a sinusoidal strain of small amplitude is applied to

the material, and the resulting stress response is measured. An important advantage of SAOS measurement is its high accuracy and reproducibility, as data are collected over multiple oscillation cycles and averaged to reduce experimental noise [3].

Furthermore, since the imposed strain remains sufficiently small, the material response lies within the linear viscoelastic (LVE) region. In the LVE region, stress is directly proportional to strain, the principle of additivity of the stress applies, meaning the effect of two strains is directly the sum of these two effects. Properties can then be derived from primary measurements. For example, the complex viscosity (η^*) can be calculated from the complex modulus through Equation 2.1 and provide a frequency-dependent measure of the material's resistance to flow. Experiences done within the LVE regime also ensures that the material structure is not disrupted during testing and that the measured response truly reflects intrinsic molecular relaxation mechanisms [3], [4].

$$\eta^* = \frac{G^*}{\omega} = \frac{G' + iG''}{\omega} \tag{2.1}$$

In the LVE region polymer melts typically display characteristic behavior for SAOS measurements. At low frequencies, they exhibit terminal behavior, where G' follows a slope of two and *G"* displays a slope of one with respect to frequency, and G'' is generally higher than G'. The viscosity often shows a Newtonian plateau at low frequency before decreasing at higher frequency. At higher frequencies, G' can exceed G'', indicating elastic dominance. The transition between these regimes corresponds to the material's characteristic relaxation times, which are strongly affected by molecular weight, molecular weight distribution, chain architecture, and intermolecular interactions [3].

Various viscoelastic models can be fitted to experimental rheological data in order to describe the material response over a wide range of shear rates or frequencies. Among the most used models are the Power Law model, the generalized Maxwell model, and the Carreau-Yasuda model. While the Power Law model is typically applied to characterize shear-thinning behavior in the non-

Newtonian regime, and the generalized Maxwell model is used to represent the relaxation spectrum of the material, the Carreau-Yasuda model provides a continuous description of the transition from the Newtonian plateau to the shear-thinning region [4], [5].

A widely used model in polymer blend rheology is the Palierne model. This model describes the linear viscoelastic response of a binary blend with emulsion type morphology. In this model, the viscoelastic moduli of the blend are expressed as a function of the matrix and dispersed phase properties, the droplet volume fraction, and the interfacial tension, as can be seen in Equation 2.2. By fitting experimental SAOS data to the Palierne model, it is possible to estimate the interfacial tension between immiscible polymers. The model assumes small deformations and negligible phases interactions, such as coalescence and breakup, making it particularly suitable for analysis within the linear viscoelastic region [6].

$$G_B^*(\omega) = \frac{1 + 3\sum_i \phi_i H_i^*(\omega)}{1 - 2\sum_i \phi_i H_i^*(\omega)} G_M^*(\omega) \tag{2.2}$$

where

$$H_i^*(\omega) = \frac{4\left(\frac{\alpha}{R_v}\right)[2G_m^*(\omega) + 5G_d^*(\omega)] + [G_d^*(\omega) - G_m^*(\omega)][16G_m^*(\omega) + 19G_d^*(\omega)]}{40\left(\frac{\alpha}{R_v}\right)[G_m^*(\omega) + G_d^*(\omega)] + [2G_d^*(\omega) + 3G_m^*(\omega)][16G_m^*(\omega) + 19G_d^*(\omega)]} \tag{2.3}$$

ϕ is the volume fraction of the dispersed phase, R_v is the average radius in volume of the dispersed droplets, α the interfacial tension, $G_B^*(\omega)$, $G_m^*(\omega)$ and $G_d^*(\omega)$ the complex modulus of the blend, the matrix and the dispersed phase respectively.

There also exist models that can describe miscible polymer blends, such as the mixing rule. This equation assumes ideal mixing behavior and no intermolecular interactions. Deviation from this law is a sign of immiscibility. As expressed in Equation 2.4, the viscosity of the blend η_b, is calculated as the sum of the viscosities of the individual neat polymers multiplied by their corresponding weight fraction w [7], [8].

$$\log \eta_b = w_d \log \eta_d + (1 - w_d) \log \eta_m \tag{2.4}$$

Other techniques can be used than model fitting to predict and understand the viscoelastic behavior of polymers and polymers blends. The relaxation time spectrum $H(\lambda)$ is a representation of the distribution of relaxation process in linear viscoelastic materials. Unlike discrete set, the relaxation spectra is a continuous function of relaxation. It is particularly relevant to calculate because of its high resolution, which allows to distinguish materials more accurately than other viscoelastic functions. The relaxation time spectrum cannot be measured directly, but it can be reconstructed from SAOS measurements using numerical inversion techniques or model-based approaches, such as the generalized Maxwell model. The relaxation time spectra $H(\lambda)$ is related to the relaxation modulus $G(t)$ by Equation 2.5. The relationship between the relaxation spectra and the loss and storage moduli are given by Equations 2.6 and 2.7. By reconstructing the relaxation behavior from SAOS data, it becomes possible to interpret the material response [5], [9].

$$G(t) = \int_{-\infty}^{\infty} H(\lambda)\, e^{-\frac{t}{\lambda}} d log\lambda \tag{2.5}$$

$$G'(\omega) = \int_{-\infty}^{\infty} H(\lambda) \frac{\lambda^2 \omega^2}{1 + \lambda^2 \omega^2} d log\lambda \tag{2.6}$$

$$G''(\omega) = \int_{-\infty}^{\infty} H(\lambda) \frac{\lambda \omega}{1 + \lambda^2 \omega^2} d log\lambda \tag{2.7}$$

Polymer relaxes over broad time ranges that are indicative of important microstructural information. Fast relaxation time are usually associated with smaller relaxation process such as small molecules and inversely, longer relaxation time are typically linked to slow, large-scale chain dynamics [10]. Relaxation spectra are therefore useful to analyse the viscoelastic behavior of

polymers and can also provide insight on the miscibility of polymer blends. Immiscible systems often exhibit additional relaxation processes to their neat phases, associated with interfacial tension contributions [6], [11].

Rheological properties are highly sensitive to molecular architecture and intermolecular interactions. Rheology is therefore a powerful tool not only to evaluate the processability and properties of a polymer, but also to investigate miscibility and phase behavior in polymer blends. Changes in relaxation dynamics, deviations from terminal behavior, or the appearance of additional relaxation modes may indicate immiscibility, interfacial effects, and phase separation.

2.2 PLA Structure and Synthesis

Polylactic acid (PLA) is a bio-based polymer, meaning that it is synthesized from natural resources rather than from petrochemical feedstock. The polymerization of lactic acid begins with the synthesis of lactic acid (LA), regardless of the polymerization route chosen. LA is the base monomer of polylactic acid. It contains both a hydroxyl and a carboxylic acid functional group, and its asymmetric carbon bearing the methyl group gives rise to two enantiomeric forms, L- and D-lactic acid, thereby making it a chiral molecule. The enantiomers of LA units are presented in Figure 2.1

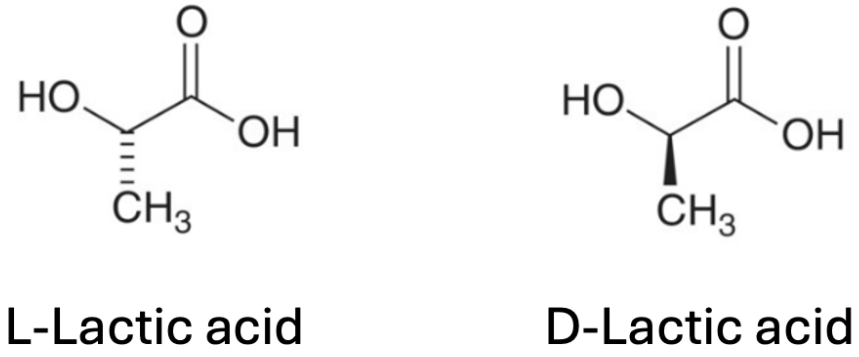

Figure 2.1 Lactic Acid Enantiomers adapted from [2]

Lactic acid can be synthesized via a catalytic route. However, this method is less favored because it requires petrochemical feedstock and produces racemic lactic acid, i.e., an equal mixture of the D- and L-enantiomers [2]. The majority of lactic acid is therefore produced via fermentation. This method is preferred due to the possibility of using biowaste as a substrate, its lower energy demand, and the ability to select the enantiomer produced through the choice of microorganisms, thereby influencing the eventual properties of the PLA formed, among other factors [12], [13].

Lactic acid can be produced from carbohydrates, i.e., from various biomass sources. Table 2.1 presents some examples of substrate sources, the types of biomass that can be used to produce LA via fermentation. The choice of biomass source directly affects the lactic acid production yield and determines the type of pretreatment required.

Table 2.1 Example of substrate for the fermentation of lactic acid adapted from [12]

Substrate Type	**Substrate**	**Pretreatment**
Starch	Sugarcane molasses	Filtration
	Potato vinasse waste and sugar beet molasses	N/A
	Sugarcane molasses and corn steep liquor powder	Acid pretreatment
Lignocellulose	Corn residues	Grinding and alkaline pretreatment
	Beech wood	Organosolv pretreatment and enzymatic hydrolysis
Dairy industry waste	Whey	N/A
	Whey powder	Enzymatic hydrolysis

Subsequently, lactic acid undergoes condensation reactions to form low-molecular-weight oligomers. Oligomers can then be polymerized to yield lactide, the cyclic dimer used for ring-opening polymerization (ROP) of PLA. Again, due to the chiral nature of the LA unit, the cyclic dimer formed (lactide) can exhibit three possible stereoisomeric configurations: L-lactide, D-lactide, and meso-lactide. ROP allows control over chain tacticity by selecting the lactide isomer used, which directly affects the polymer's crystallinity and properties, and is therefore the preferred route for producing high molecular weight polymers [14]. Polymerization can be carried out in different media (melt, solution, suspension, bulk), with the choice of medium affecting viscosity, reaction yield, and processing conditions [15]. Post-treatment steps such as drying are commonly performed but will not be considered here due to their variability.

Most industrial processes use L-lactide to produce isotactic PLLA, which is highly crystalline and exhibits superior properties [16]. Similarly, polymerization of D-lactide yields isotactic PDLA. In contrast, polymerization of a racemic mixture of L- and D-lactide produces poly(D,L-lactide) (PDLLA), while meso-lactide leads to the formation of poly(meso-lactide) (PMLA) (see Figure 2.2). Due to their stereoirregular backbone structure, both PDLLA and PMLA are unable to

crystallize efficiently and are therefore typically amorphous. As a result, they exhibit thermal and mechanical properties that differ significantly from those of stereoregular PLA [17].

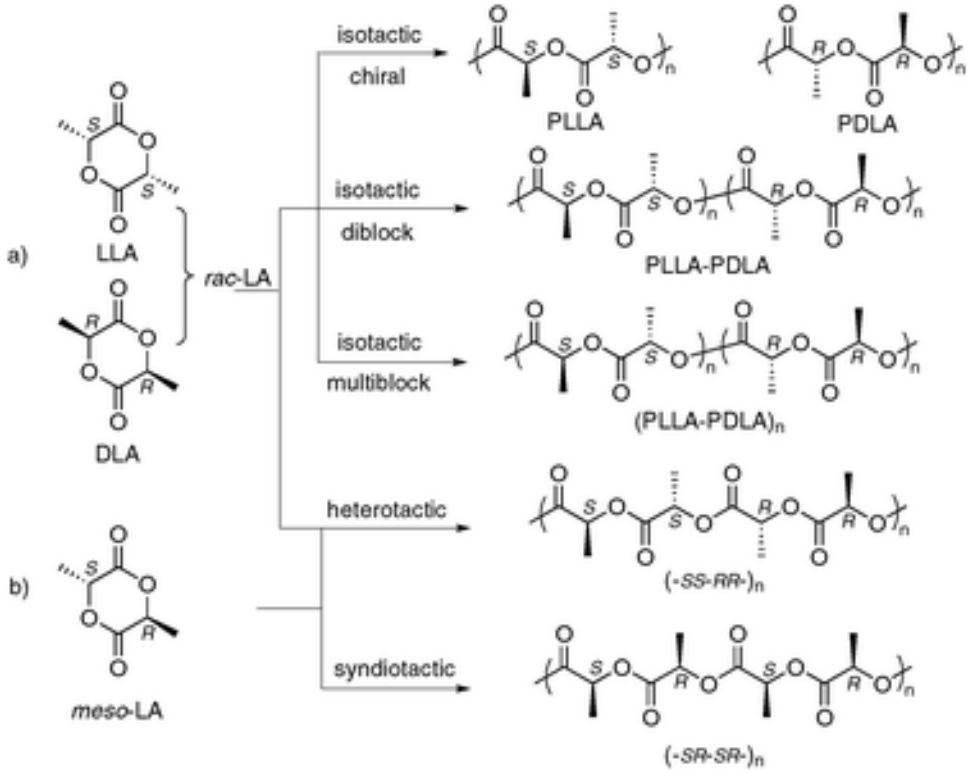

Figure 2.2 PLA obtained from ROP of (a) rac-lactide and (b) meso-lactide reproduced from [18]

2.3 PLA Properties

2.3.1 PLA Thermal Properties

PLA thermal properties are strongly dependant on its tacticity. An isotactic PLA, like PLLA or PDLA, will have regular polymer chains, increasing the crystallinity of the polymer, resulting in a semi-crystalline polymer [19]. On the contrary, an atactic PLA, such as PDLLA or PMLA, will have a stereoirregular backbone, generally resulting in an amorphous [17].

Semi-crystalline PLA therefore displays a crystallization temperature (T_c) during cooling, as well as a melting temperature (T_m) and a cold crystallization temperature (T_{cc}) during heating, whereas amorphous PLA does not show these crystallization transitions. The melting temperature of

isotactic PLA typically ranges between 170 and 190 °C, whereas randomly optical PLA $_{Tm}$ ranges from 130-170 °C [20]. Crystallisation temperatures are generally observed in the ranges of 100–160 °C, while the degree of crystallinity of PLA widely varies, ranging from nearly amorphous to about 35%, depending on processing conditions and molecular characteristics [21]. PLA's crystallinity is influenced by several factors, such as molecular weight, stereoregularity, and thermal history. An increase in stereoregularity results in a more regular polymer backbone, which promotes crystal formation and consequently increases both T_c and T_m [22].

The tacticity of PLA also affects its glass transition temperature (T_g) as it increases with the stereoregularity of PLA [22], [23]. Amorphous PLA typically exhibit a T_g in the range of 45-55 °C, whereas semi-crystalline PLA ranges up 65°C [20]. The values of T_g increases with crystallinity, as crystalline domains hinder the movement of amorphous polymeric chains. The T_g values of amorphous PLA are therefore always lower than those of a semi-crystalline PLA.

Stereoregularity is not the only factor that influences the thermal transitions of PLA, its T_g, T_m and T_{cc} generally increases with molecular weight. The intrinsic viscosity of PLA increases exponentially with molecular weight, making the polymeric chains less mobile and leading to higher transition temperatures. Furthermore, the higher viscosity caused by the increase in molecular weight makes the diffusion process more difficult during crystallisation. Consequently, a lower molecular weight PLA typically crystallizes more rapidly than a higher molecular PLA. Therefore, crystallisation occurs at a higher T_c during cooling, while T_{cc} decreases during heating because of the greater chain mobility for lower molecular weight PLA. This behavior may also lead to higher apparent crystalline content, just as observed by Pan et al. (2007) for PLLA [24].

These thermal characteristics are particularly important for melt processing and rheological behavior, as chain mobility above T_g and structural organization near T_c and T_m directly influence viscoelastic response and processing temperatures. However, PLA's processing is limited by its thermal stability. PLA is thermally unstable, with degradation initiating at relatively low processing temperatures, around 200 °C [25]. This thermal degradation leads to a decrease in PLA's molecular weight, affecting its mechanical and rheological properties. In addition, elevated temperatures and

shear stresses further accelerate degradation, thereby limiting its processing window and the reliability of rheological measurements [26], [27]. The thermal stability of PLA is also influenced by several structural parameters, including tacticity, molecular weight, and degree of crystallinity [28]. PLA's thermal resistance increases with crystallinity, as crystalline regions restrict chain mobility and therefore delay the thermal degradation [29]. Furthermore, Yang et al. (2025) found that lower molecular weight semi-crystalline PLA exhibited better thermal stability [30], which may be associated with the increase of cold crystallisation for lower molecular weight [28], [31]. They also reported that the activation energy of thermal degradation decreases with increasing molecular weight [30].

2.3.2 PLA Mechanical Properties and Applications

PLA is one of the most widely used alternatives to petrochemical-based plastics due to its biodegradability, which is why it is primarily employed in the packaging sector [32]. In addition, PLA exhibits notable mechanical properties, with a higher elastic modulus and tensile strength than polypropylene (PP) and high-density polyethylene (HDPE) [33]. PLA is also biocompatible, making it well-suited for biomedical applications. Its ability to absorb organic compounds, combined with its capillary properties, has further enabled its use in the fibers and textiles industry [32]. Some common applications of PLA are summarized in Table 2.2.

Table 2.2 Common applications of PLA based on [32]

Application Area	**Example of applications**
Packaging	Plastic bottles, yogurt cups
Agriculture	Protective films against insects and climate
Textile and Fibers	Wipes, masks
Biomedical Applications	Drug delivery systems, scaffolds for bone tissue engineering, medical implants

2.3.3 PLA Rheology

PLA has been the subject of numerous research recently, mainly for its biodegradable nature and potential as a sustainable alternative to petroleum-based polymers. PLA is widely used in applications such as fibers and packaging, and is often processed in the molten state [2]. It is therefore important to understand its melt rheological behavior. In the melt, PLA behaves as a viscoelastic polymer whose response depends strongly on molecular weight, temperature, stereochemistry, and thermal history.

An important consideration for PLA melt rheology is its thermal stability, as extended exposure to high temperatures can induce molecular weight degradation, altering the measured rheological response. This limits certain experiments such as time–temperature superposition to a narrow temperature range, as measurements need to be above the melt temperature and stay underneath the degradation temperature [23]. This also makes it more difficult to reach lower frequency during frequency sweep measurements, as these experiments require longer measurement times and therefore increase the risk of thermally degrading PLA.

PLA exhibits typical linear viscoelastic behavior of polymer melts. In small-amplitude oscillatory shear experiments, PLA generally shows a terminal flow region at low frequencies, its storage modulus follows a slope of 2 and its loss modulus follows a slope of one. At higher frequencies, the moduli reach a crossover points, and elastic moduli dominates. The complex viscosity of PLA presents typical shear-thinning behavior, decreasing as shear rate increases. It also presents a clear Newtonian plateau at low frequency [34].

The rheological properties of PLA are strongly influenced by molecular weight, such as the zero-shear viscosity [35]. Dorgan et al. (1999) found that the zero-shear viscosity of PLA increases with the 4.6 power of its molecular weight [34]. Therefore, even moderate reductions in molecular weight due to thermal degradation or hydrolysis can significantly decrease melt viscosity. PLA's storage and loss moduli also decreases with a decrease in its molecular weight. Pan et al. (2007)

studied PLA blends low and high molecular weight and concluded that the rheological properties of the blends all decreased with the increase of low molecular weight PLA content [24], [36].

Stereochemistry also influences the melt rheology of PLA. The fraction of D-lactide in the polymer chain can influence crystallization, chain packing, and molecular mobility. Increasing the D-lactide content of PLA generally disrupts the regularity of the polymer chains, which can affect not only the thermal but also the rheological properties of the material. An increase in stereo purity generally increases PLA's viscosity. Dorgan et al. (2005) found that the plateau modulus of PLA varied within a range of about 20% with optical composition [23].

2.4 Polymer Blends

Polymer blends are an economical and versatile way to obtain new materials with tailored properties without the need to synthesize entirely new polymers. By combining existing polymers, it is possible to adjust mechanical, thermal, rheological, and degradation behaviors in a relatively straightforward and scalable manner. Polymer blends not only create new material, but they also are a powerful tool to investigate polymer behavior, such as chain interactions, relaxation dynamics, crystallization behavior, and degradation mechanisms. They offer insight on how molecular structure translates into macroscopic performance.

However, only a limited number of polymer blends are made of miscible components, most polymer blends are thermodynamically immiscible. For a polymer blend's components to be miscible, the free energy of mixing ΔG_{mix} must be negative, ensuring mixing is spontaneous. Equation 2.8 is the definition of Gibbs free energy applied to blends. Miscibility between components therefore requires either a sufficiently negative enthalpy of mixing ΔH_{mix}, or an entropic contribution S_{mix} large enough to overcome a positive enthalpy term. In practice, ΔH_{mix} is normally positive for polymer blends due to unfavorable intermolecular interactions and S_{mix} is normally small due to the high molecular weight of polymer which limits the entropy gain upon mixing. As a result, the free energy of mixing remains positive in most cases, leading to immiscibility [37].

$$\Delta G_{mix} = \Delta H_{mix} - TS_{mix} \tag{2.8}$$

Immiscible polymers separate into distinct phases rather than forming a single homogeneous phase in order to minimizes the system's free energy. Phase separation can occur through different mechanisms, such as spinodal decomposition or nucleation and growth. Spinodal decomposition is characterized by an interconnected structure that spontaneously and continuously separates, while nucleation and growth by small domains of one phase that form and progressively expand over time. Phase diagrams are a useful tool to visually represent the thermodynamic conditions at which these decompositions occur. An example of a phase diagram is presented in Figure 2.3. Inside the binodal curve, the material present two distinct phases, while outside of this curve the material present one phase. Between the spinodal and binodal curves, the material is in the metastable region. The blend is biphasic, but phase separation occurs via nucleation and growth mechanism rather than by spinodal decomposition. These mechanisms lead to the development of a heterogeneous morphology characterized by dispersed domains or co-continuous structures [38].

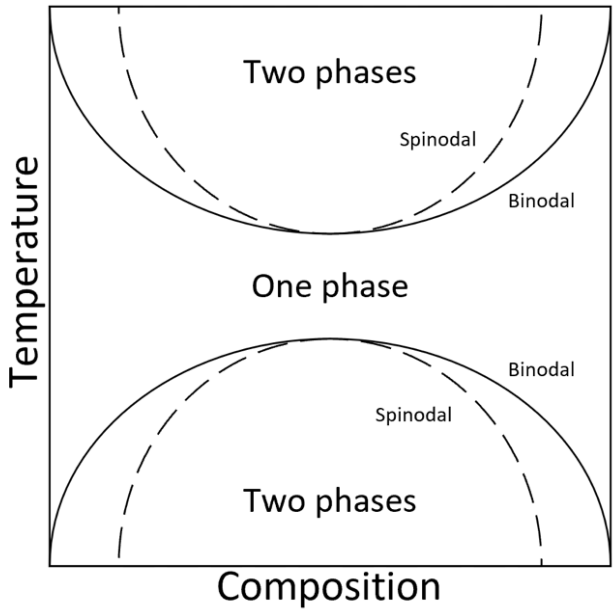

Figure 2.3 Phase diagram of LCST AND UCST blends based on [39]

Immiscible blends being prevalent, compatibilization is often required to enhance interfacial adhesion and stabilize the morphology. Compatibilization of blends aim to reduce the interphase, region that separates the polymer phases. It plays a critical role in governing the mechanical performance, rheological behavior, and long-term stability of the blend. Quantifying the degree of immiscibility, particularly through measurements of interfacial tension and morphological analysis, is therefore essential to understand and control blend properties.

PLA has been widely blended with various polymers, including both biodegradable and non-biodegradable materials, as well as bio-based and petroleum-based polymers. The primary objective of these blends is often to overcome some of PLA's drawbacks, such as its relatively slow biodegradation rate in certain environments and its limited mechanical performance, such as its brittleness. PLA has been blended with several biodegradable polymers, including starch, chitosan, polycaprolactone, and poly(butylene succinate), often to enhance flexibility or biodegradability. In addition, blends with petroleum-based polymers such as polyethylene, polypropylene, polystyrene, polyamide, and poly(methyl methacrylate) (PMMA) have also been investigated to improve mechanical properties, thermal resistance, or processability. However,

most PLA blends are thermodynamically immiscible, leading to phase-separated morphologies, although miscibility has been reported in some systems, such as PLA/PMMA blends [40], [41].

Some studies have also investigated binary blends of different PLA grade, such as different molecular weight, tacticity, branching. Most of the literature focuses on blends of PLLA with PDLA, which can form stereocomplex crystals, when mixed with an equimolar ratio. The formation of stereocomplex crystals is known to results in materials with different properties than their homopolymers, such as higher crystallinity, higher transition temperatures, improved thermal stability and higher viscosity [42], [43], [44].

Other studies have examined PDLLA and PLLA blends in order to understand the impact of PDLLA on PLLA's crystallinity and their miscibility. In particular, Pan et al. (2009) found that PLLA and PDLLA were miscible at all compositions, and that PDLLA affected the crystalline structure of PLLA [45]. The miscibility of the blend was evaluated by studying blend crystallinity only. Tsuji and Ikada (1996) studied the impact of the varying molecular weight of PDLLA on the crystallisation behavior and morphology of PLLA by solvent blending equimolar blends of both PLAs. They found that the blends crystallinity was the highest for lower molecular weight PDLLA, and that the crystalline structure was more ordered for the lower molecular weight PDLLA. They also concluded that the two components were miscible, as PDLLA disrupts PLLA crystallization, implying intimate contact between the phases [46].

However, the literature is not unanimous regarding the miscibility of PDLLA and PLLA, as previous conclusions were based solely on crystallinity results. Bouapao et al. (2009) reported immiscibility for PLLA and PDLLA blends at intermediate compositions (PLLA = 0.3–0.9), evidenced by the presence of two glass transition temperatures associated with the neat phases. They also showed that the presence of amorphous PDLLA reduces the crystallization rate of PLLA, while the crystalline structure remains identical to that of neat PLLA, indicating that PDLLA hinders crystallization kinetics without altering the crystal form [47]. Chen et al. (2003) also found PLLA and PDLLA to have poor miscibility. They observed two distinct T_g via DSC for all

composition tested, 80%, 60%, 50%, 40% and 20%, but concluded the addition of a surfactant could yield better miscibility, making PLLA tougher [48].

These studies aim to understand the effects of different blends on crystallization behavior, miscibility, rheological properties, etc. [23], [30], [34], [35]. However, blends involving PMLA with any PLA have not yet been reported in the literature, highlighting a gap in current research.

CHAPTER 3 OBJECTIVES

3.1 Objectives

This work aims to better understand the melt rheological and thermal behavior of PMLA by using PLLA as a well-characterized reference polymer in binary blends. The objectives of this work are to:

- Investigate the thermal properties of neat PMLA and PLLA, as well as their binary blends, using differential scanning calorimetry.
- Characterize the melt rheological behavior of PMLA, PLLA, and PLLA/PMLA blends under small-amplitude oscillatory shear.
- Investigate the morphology of PLLA and PMLA blends and establish correlations between phase morphology and rheological behavior.
- Analyze the miscibility and phase behavior of PLLA/PMLA blends through thermal and rheological indicators, such as model fitting and relaxation spectra.

The main results are presented in the form of a scientific article in the next chapter.

CHAPTER 4 ARTICLE 1: MORPHOLOGICAL, THERMAL AND RHEOLOGICAL BEHAVIOR OF POLY(L-LACTIDE) AND POLY(MESO-LACTIDE) BLENDS

Maude SICOTTE-BRISSON[1], Patricia MORAILLE[2], Jed RANDALL[3], Marie-Josée DUMONT[4], Pierre CARREAU[1], Marie-Claude HEUZEY[1]

Article submitted to the Journal of Rheology on April 2nd 2026

Author Contributions

Maude Sicotte-Brisson: Conceptualization, Data Curation, Formal Analysis, Investigation, Methodology, Visualization, Validation, Writing/Original Draft Preparation, Writing/Review & Editing. **Patricia Moraille:** Conceptualization, Data Curation, Formal Analysis, Investigation, Methodology, Visualization, Validation, Writing/Original Draft Preparation, Writing/Review & Editing. **Jed Randall:** Resources, Validation, Writing/Review & Editing. **Marie-Josée Dumont:** Supervision, Validation, Writing/Review & Editing. **Pierre Carreau:** Supervision, Validation, Writing/Review & Editing. **Marie-Claude Heuzey:** Funding Acquisition, Project Administration, Resources, Supervision, Validation, Writing/Review & Editing.

4.1 Abstract

Polylactide (PLA) is one of the most widely studied biodegradable polymer. However, poly(meso-lactide) (PMLA), an amorphous PLA, remains poorly characterized. This study investigates the thermal, rheological behavior, and morphology of poly(L-lactide) (PLLA) and poly(meso-lactide) blends across a wide composition range. Characterizations were performed using differential scanning calorimetry (DSC), small amplitude oscillatory shear (SAOS) rheology, and atomic force microscopy (AFM). Partial miscibility is suspected for the 10% and 90% w/w% $_{HMW}$ PLLA/ $_{HMW}$ PMLA compositions, while 30 w% $_{HMW}$ PLLA, 50 w% $_{HMW}$ PLLA and 70 w% $_{HMW}$ PLLA

[1] CREPEC, Department of Chemical Engineering, Polytechnique
[2] Department of Chemistry, Université de Montréal, Montréal, QC, Canada
[3] NatureWorks LLC, Plymouth, MN, USA; current affiliation Jed Randall Consulting LLC, Minneapolis, MN, USA
[4] CREPEC, Department of Chemical Engineering, Université Laval, Québec, QC, Canada

compositions exhibited immiscibility. DSC revealed two glass transition temperatures for immiscible blends, corresponding to those of the neat phases, 48.2 ± 0.1 °C for $_{HMW}$PMLA and 61.8 ± 0.4 °C for $_{HMW}$PLLA, and a single T_g for partially miscible blends. AFM revealed an emulsion-type morphology at 30 wt% and 70 wt% $_{HMW}$PLLA compositions, and a co-continuous structure at 50 wt% $_{HMW}$PLLA. SAOS results presented a shoulder in the low frequency storage modulus for immiscible blends, and a slight shoulder for partially miscible blend. The Palierne model was used to fit the dynamic data of the immiscible compositions and estimated the dispersed phase relaxation time, reinforcing the immiscibility conclusions. Cole-Cole plots and relaxation spectra were obtained for all blends, showing two distinct relaxations modes for immiscible ones. These results suggest that PMLA and PLLA are immiscible at intermediate compositions, with hypothesized partial miscibility at low and high PLLA contents.

Keywords: Polymer Blends, Poly(L-lactide), Poly(meso-lactide), Atomic Force Microscopy, Small Amplitude Oscillatory Shear, Palierne model

4.2 Introduction

Fossil-based polymers are widely used across numerous applications, yet they place considerable stress on the environment throughout their production and their disposal [1]. As a result, numerous efforts have recently been put towards research on biodegradable and biosourced polymers, including polylactide (PLA), a now well-known biobased aliphatic polyester. Because of its interesting mechanical properties, including high modulus and tensile strength, PLA is used in many different applications, such as medical devices, textiles and fibers and packaging [32]. PLA offers a promising opportunity to reduce the environmental footprint associated with conventional plastics.

PLA is primarily obtained via ring opening polymerisation of lactide, a cyclic dimer of lactic acid that exists in three different isomers, L-Lactide, D-Lactide and meso-Lactide, as seen in Figure 1 [49]. The physical and mechanical properties of the resulting PLA are strongly influenced by the stereochemistry of the lactide feed [50]. A feed predominantly consisting of L-Lactide or D-Lactide will form a crystalline polymer, while a racemic mixture of L-Lactide and D-Lactide (commonly referred to as DL-lactide or rac-lactide) or a feed mainly composed of meso-lactide will form an

amorphous polymer [17]. Glass transitions temperatures varies with this stereo structure, increasing with stereo purity and also crystallinity [23]. Amorphous PLA have a glass transition temperature (T_g) that ranges from 45 to 55 °C, while the T_g of semi-crystalline PLA can go up to 65 °C [20]. The rheology of PLA is also affected by its stereochemistry, as it impacts the chain regularity, packing, and characteristic ratio, or chain stiffness, which in turn affect the chain mobility of the polymer. The zero-shear viscosity and viscoelastic moduli are therefore higher for stereoregular PLA compared to stereoirregular PLA at equivalent molecular weight [17].

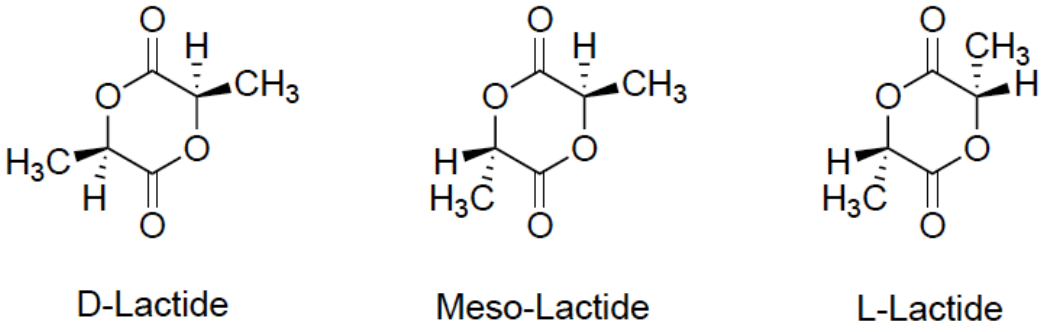

Figure 4.1 The three lactides isomer based on Groot *et al.* [49]

Poly(meso-lactide) (PMLA), a polylactide synthesized from meso-lactide, has only recently emerged as a potentially interesting PLA [17]. While PMLA shares structural similarities with PLLA, it can be expected to degrade faster than crystalline PLA as it is amorphous and has a lower T_g [51], [52], [53] and displays distinct thermal and rheological behaviors [17]. Randall *et al.* [17] reported that PMLA synthesised from meso-lactide is highly stereoirregular with short block lengths, resulting in a more flexible chain structure than stereoregular PLLA. Moreover, PMLA remains poorly understood. Blending PMLA with PLLA could thus be a promising approach to further understand its potential and its differences from other PLA types, especially given the processing challenges and degradation sensitivity of PLLA. The incorporation of PMLA could prove to be an attractive strategy to modulate the rheological and mechanical performance of PLLA-based blends. Not only this approach could potentially accelerate PLLA's degradation but also help alleviate the current technical challenges that impede the widespread industrial

application of poly(L-lactide) (PLLA), including its characteristic brittleness, limited thermal resistance, and suboptimal barrier properties.

In this article, the morphological, rheological and thermal behavior of PMLA/PLLA blends are investigated over a wide composition range. Immiscible and suspected partially immiscible blends morphologies are imaged via atomic force microscopy (AFM). Small amplitude oscillatory shear (SAOS) data are obtained for the PLAs and their blends. SAOS data are fitted with two different emulsion type models. The miscibility or immiscibility of the blends is further investigated through the relaxation time spectrum analysis, as well as from differential scanning calorimetry data.

4.3 Material and methods

4.3.1 Materials

Four grades of PLA were supplied by NatureWorks LLC™ (Table I), including two PLLA and two PMLA grades. Each polymer type was represented by one lower and one higher molecular weight sample, enabling direct comparison at matching molecular weight levels.

Table 4.1 Nomenclature, molecular weight and D-lactide content of the four different grades of PLA

Polymer Type	Grade	Description	Molecular Weight M_n (kg/mol)	D-Lactide content (%)
$_{HMW}$PLLA	Ingeo 2500HP	High Molecular Weight ($_{HMW}$)	194	0.5
$_{LMW}$PLLA	Ingeo 6100D	Low Molecular Weight ($_{LMW}$)	115	0.4
$_{HMW}$PMLA	752-27-01	High Molecular Weight ($_{HMW}$)	195	44.7
$_{LMW}$PMLA	752-27-02	Low Molecular Weight ($_{LMW}$)	135	45.1

4.3.2 Preparation of samples

PLA pellets were dried overnight in a vacuum oven at 40 °C prior to processing. The samples were blended at 190 °C in an internal HAAKE™ Rheomix OS mixer (Thermo Scientific, USA) under a nitrogen atmosphere, with a roller rotor at a speed of 50 RPM for 15 minutes. PLLA of high and low molecular weight were blended respectively with 10, 30, 50, 70 and 90 %wt/wt of PMLA of high or low molecular weight. The resulting blends were then molded in a hot press at 190 °C under nitrogen atmosphere to form disks with a diameter of 25 mm and a thickness of approximately 1.5 mm. Neat polymers were subjected to the same preparation for comparison purposes.

Prior to AFM, samples were blended and pressed into disks as described, then rapidly quenched with ice. Samples were then sliced in a Microtome MT990 with CR1000 (RMC Boeckeler, Singapore).

4.3.3 Measurements

AFM

As outlined in the Materials and Methods section, all samples were subjected to microtoming prior to atomic force microscopy (AFM) characterization. The morphology of the blends of $_{HMW}$ PLLA and $_{HMW}$ PMLA was investigated using AFM, as scanning electron microscopy (SEM) could not provide sufficient contrast. Both polymers are chemically similar, differing only in stereochemistry, which does not produce detectable contrast in SEM. AFM, however, revealed contrast by highlighting the difference in nanomechanical properties of both PLA phases and AFM-IR provided unequivocal differentiation and effective identification of each PLA phase.

Surface topography and qualitative nanomechanical contrast AFM images were acquired in ambient conditions using a NanoScope® 6 controlled-Dimension ICON atomic force microscope equipped with a Lakeshore temperature controller (Bruker, Santa Barbara, CA, USA). Images were acquired while operating in two imaging modes: PeakForce QNM and Phase Imaging Tapping

Modes. These surface characterization techniques were instrumental in visualising the morphology of each blend, as well as unravelling the fine nanometric phase structure of each phase.

Quantitative Nanoscale Mechanical AFM Characterization (PeakForce QNM®)

Topography and qualitative nanomechanical AFM images were acquired using the PeakForce QNM® Tapping mode. During the scan, force-distance curves are acquired off-resonance at a 2kHz rate and with a constant imaging force (Peak Force Setpoint) of 1500-2200 picoNewton while heating the sample stage at 50 °C. A contrast in the mechanical properties of $_{HMW}$ PLLA and $_{HMW}$ PMLA phases is expected at 50 °C as $_{HMW}$ PMLA glass transition temperature is below this temperature, whereas $_{HMW}$ PLLA is higher. We used RTESPA-330 aluminum coated, etched silicon probes with rotated tips (8 nm nominal tip radius, res. freq. 300 ± 100 kHz, spring constant k = 40 N/m) manufactured by Bruker. Force curve processing was conducted in real time in order to extract nanomechanical property mapping channels.

Data obtained from the height, dissipation, and indentation channels are presented. The height channel maps surface topography, and the dissipation channel quantifies the energy lost during the tapping cycle to viscoelastic interactions (largely due to viscous, inelastic deformation). Finally, the indentation channel maps the indentation depth the tip produced into the sample [54]. The DMT modulus channel, which indicates local stiffness and is calculated using the DMT model [54], was excluded because the contrast obtained was systematically inverted for all blends. The contrast inversion observed for the DMT modulus channel is likely attributable to a combination of the DMT model's limitations and the complexity of the tip–sample contact interaction. Consequently, this article exclusively focuses on the dissipation and indentation channels for the interpretation of nanomechanical phase behaviour.

TappingMode PhaseImaging™ AFM Characterization

The topography and phase images were acquired using TappingMode PhaseImaging™ at room temperature with a probe manufactured by Bruker (model: RTESPA-525A, aluminium-coated, etched silicon probes with rotated tips and a nominal tip radius of 8 nm, resonance frequency of

525 ± 150 kHz and spring constant of 200 N/m). Throughout the scan, oscillating damping of approximately 20% was applied. Phase imaging simultaneously maps topography (height sensor channel) and material's viscoelastic behavior (phase channel). This is achieved by monitoring changes in the amplitude of an oscillating cantilever as a *z*-feedback loop constantly adjusts the piezo scanner's position in *z* to track the sample surface while simultaneously mapping the phase lag of the periodic signal driving the cantilever. The phase lag exhibited by the cantilever is indicative of disparities in the material's viscoelastic properties [55].

Resonance enhanced AFM-IR

IR spectra and IR maps were collected at ambient conditions on microtomed samples by means of photothermal AFM-IR spectroscopy operating in the Resonance Enhanced AFM-IR [56] and operating in contact mode with a commercially available NanoIR2 (Bruker, Santa Barbara, CA, USA.). The area under the probe is illuminated by a tunable pulsed infrared quantum cascade laser (QCL) (Daylight Solutions MIRcat) with four stages covering the spectral ranges: 1909–1660, 1660-1451, 1451-1189 and 1189-911 cm^{-1} and an adjustable phase-locked loop (PLL). The absorption of infrared light excites vibrational modes localized on specific chemical groups, converting optical energy into vibrational energy. This vibrational energy initiates a thermal expansion pulse beneath the AFM tip, which is subsequently transmitted to the probe's resonance modes, which act as the local detector. The photothermal effects result in changes to the oscillation amplitude of the probe's cantilever, which is directly proportional to the sample's absorptivity. We use silicon gold coated probes model: PR-EX-nIR2-10 (20 nm tip apex diameter, res. freq. 13 ± 4 kHz, spring. const. 0.07–0.4 N/m) manufactured by Bruker. The repetition rate for the QCL laser was set to match the contact resonance mode frequency of the cantilever (typical pulse rate ≈ 180-200 kHz). The probe's motion is then measured by reflecting a laser beam off the PSD detector. Single-IR absorption spectra were acquired at the sample's surface with a 90° polarization of the IR laser light, with 128x scans co–added, laser power ≈ 1 % - 4 %, duty cycle of 10 % and spectral resolution was of 1 cm^{-1}. In order to enhance the signal-to-noise ratio (SNR), a total of 5 spectra were averaged at each point. Single point spectra were smoothed using the Savitzky-Golay method (Polynomial: 3, number of smoothing points: 5). Topographic images and AFM-IR maps were

acquired simultaneously at scan rates set to 0.5 Hz. Depending on the scan size, the resolution ranged between 10 and 100 nm per pixel.

Morphology Analysis

The mean radius in number average R_n and in volume average R_v were calculated for the blends of 30/70 %w/w and 70/30 %w/w $_{HWM}$ PLLA/$_{HMW}$ PMLA with Equations 1 and 2. The Saltikov correction was applied to account for the sample microtome cut not slicing all particle at their equator [57], [58]. The radius of the dispersed phase particles was obtained from the analysis of ten different 25 x 12.5 μm AFM images for the 30% $_{HMW}$ PLLA blend and of three different 25 x 12.5 μm AFM images for the 70% $_{HMW}$ PLLA blend composition via ImageJ software. A minimum of 25 particles per images were analysed for the 30% $_{HMW}$ PLLA blend, and 130 particles for the 70% $_{HMW}$ PLLA blend. The polydispersity I was then calculated from Equation 3.

$$R_n = \frac{\sum n_i R_i}{\sum n_i} \tag{1}$$

$$R_v = \frac{\sum n_i R_i^4}{\sum n_i R_i^3} \tag{2}$$

$$I = \frac{R_v}{R_n} \tag{3}$$

where n_i is the number of droplets with radius R_i

DSC

Differential scanning calorimetric measurements were carried on a DSC-Q2000 (TA instruments, USA) under nitrogen. Samples of approximately 15.5 ± 0.5 mg of polymer were sealed in aluminum pans. First and third scan were conducted from 30 °C to 200 °C with a heating rate of 5 °C /min. The second scan was conducted from 200 °C to 30 °C with the same cooling rate. The results were analyzed from the second and third scan via TA Instruments software. All thermograms presented were shifted vertically to clearly distinguish the different curves. A heat of

fusion for 100% crystalline polymer ΔH_m^* of 93 J/g was used to calculate the crystallinity of the samples. Equation 4 was applied for the second heating cycle and Equation 5 for the cooling cycle.

$$X = \frac{\Delta H_m - \Delta H_{cc}}{\Delta H_m^*} \quad (4)$$

$$X = \frac{\Delta H_c}{\Delta H_m^*} \quad (5)$$

where ΔH_m , ΔH_{cc} and ΔH_c are the enthalpies of melting, cold crystallisation and crystallisation.

Rheology

Rheometry was performed using a MCR-302 rotational rheometer (Anton Paar, Austria) under a nitrogen atmosphere. Tests were done with a parallel-plate stainless steel geometry with a diameter of 25 mm and a gap of 1 mm at 190 °C. Small amplitude oscillatory shear SAOS results were obtained in the linear viscoelastic regime with 10% amplitude strain over a frequency range of 0.1–628 rad/s and 628-0.1 rad/s for all blends and neat polymers. Results were then assembled to remove any data affected by PLA degradation. Data were excluded beyond 10% degradation of the complex viscosity. The degradation times for the neat polymer and the blends were determined beforehand using time-sweep measurements at a strain amplitude of 10% and a frequency of 1 rad/s. Additional lower frequencies were tested separately for the blends of 30/70 %wt/wt, 50/50 %wt/wt and 70/30 %wt/wt $_{HMW}$ PLLA / $_{HMW}$ PMLA, in the range of 0.01-0.1 rad/s and 0.1-0.01 rad/s. The same technique was used to exclude any degraded data. Relaxation spectra were calculated from the storage and loss moduli using the nonlinear regression technique NLREG [59]. Blends results are shown for the binary blend of $_{HMW}$ PLLA with $_{HMW}$ PMLA only. Other blends results can be found in the Supporting Information section.

4.4 Results and Discussion

4.4.1 Morphology Analysis

The phase morphology and composition for the different $_{HMW}$ PLLA and $_{HMW}$ PMLA blends can be visualized in the atomic force microscopy (AFM) images acquired with the PeakForce QNM mode at 50 ◦C. Note that PFQNM performed at room temperature couldn't not provide satisfying contrast between the two strereoisomers. The dissipation, indentation and height channels are presented in Figure 2. The mean radius obtain for emulsion type morphology are presented in Table II.

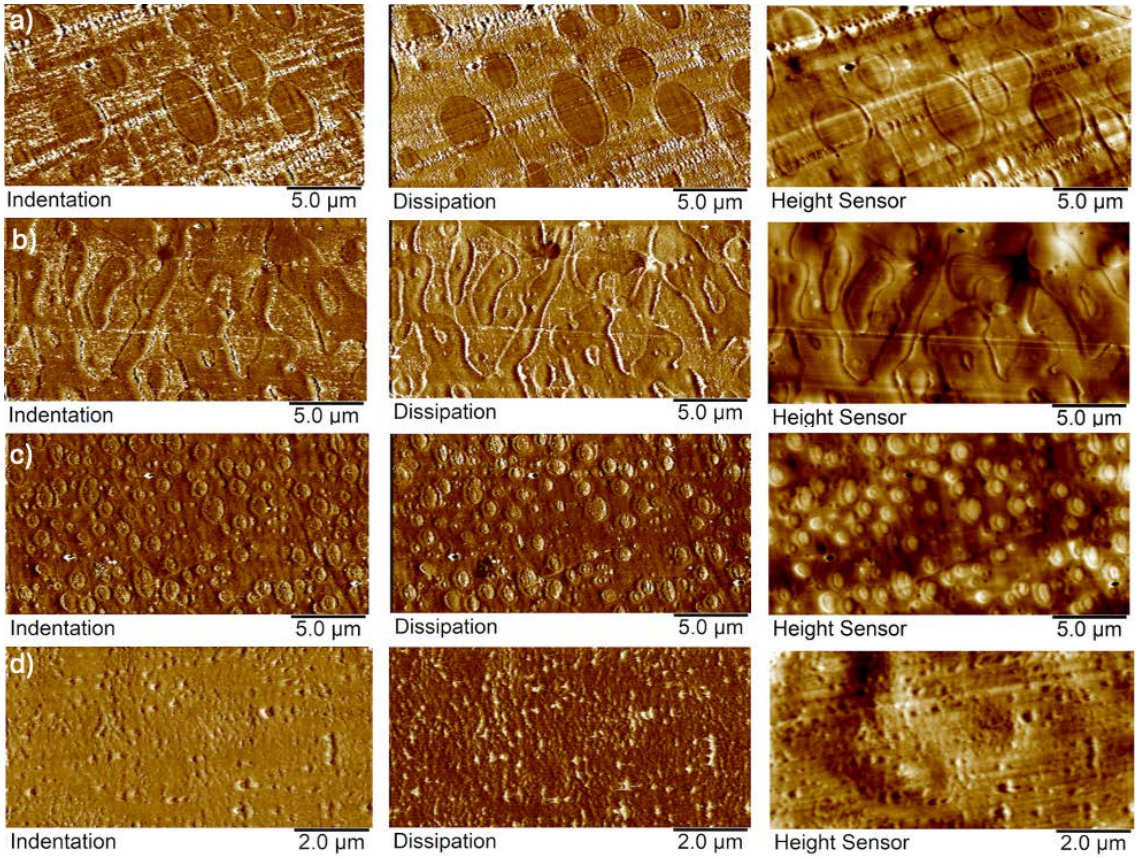

Figure 4.2 Peak Force QNM AFM images acquired at 50 °C (25 x 12.5 μm^2) of $_{HMW}$ PLLA and $_{HMW}$ PMLA blends with (a) 30 wt% $_{HMW}$ PLLA (b) 50 wt% $_{HMW}$ PLLA (c) 70 wt% $_{HMW}$ PLLA and (d) 90 wt% $_{HMW}$ PLLA content. From left to right: Indentation, Dissipation and Height Sensor maps.

Overall, the indentation channels displayed the $_{HMW}$ PMLA phase in a lighter colour, indicating that this phase had experienced greater indentation from the probe scanning at a constant force. The dissipation channels also displayed the $_{HMW}$ PMLA phase in a lighter colour. This is an

expected result, as softer materials typically exhibit higher dissipation. Compared to the semi-crystalline $_{HMW}$PLLA phase, the $_{HMW}$PMLA is amorphous and has a more flexible chain structure due to its stereoirregularity. This increased flexibility allows for greater viscous flow and structural rearrangement under the AFM tip, resulting in higher energy loss (hysteresis) during the tapping cycle. In contrast, stiffer materials show low energy dissipation because they deform elastically, returning most of the energy to the probe. The height sensor channel, which shows the sample's topography, also correlates with the phase morphology and distribution observed in the other channels. The DMT modulus channel, which maps the local stiffness is calculated using the DMT mode [54], was excluded from this discussion on the basis that the contrast obtained was systematically inverted. For all blends, the $_{HMW}$PLLA phase was darker in colour, suggesting a lower modulus than that of $_{HMW}$PMLA's. The DMT model is the continuum mechanics model that is used here to characterize the interaction between an AFM probe and the sample surface, it is an extension of the Hertzian contact model that assumes linear elasticity [60]. This assumption can lead to significant deviations from actual values as this model fails to account for viscoelastic or viscoplastic flow. For polymers that exhibit these types of behaviors or have brittle characteristics, the linear elastic premise is often invalid, resulting in modulus values that do not reflect intrinsic material properties[61]. For a rigid material, the reliability of the measured moduli decreases when the ratio of indentation depth to cantilever deflection is too low. Due to limited surface deformation, brittle materials such as $_{HMW}$PLLA could lead to fitting errors of the DMT model. Further investigating of PLA's phase deformation behavior will be needed to comprehend the obtained modulus contrast and draw conclusions about its origin; however, this is beyond the scope of the present work.

The AFM images revealed an emulsion-type morphology for the 30 wt% $_{HMW}$PLLA and 70 wt% $_{HMW}$PLLA blends and a co-continuous morphology for the 50 wt% $_{HMW}$PLLA blend, all immiscible blends morphology. In Figure 2 c), where $_{HMW}$PMLA is the dispersed phase and $_{HMW}$PLLA the matrix, the droplets are smaller than those observed in Figure 2 a). This difference can be attributed primarily to the viscosity ratio between the two phases, which is defined as the ratio of the dispersed phase viscosity over the matrix viscosity ($\kappa = \eta_d/\eta_m$) [62]. In image c), $_{HMW}$PLLA exhibits a higher viscosity than $_{HMW}$PMLA, therefore $\kappa < 1$ and the matrix can transfer the flow more effectively to the dispersed phase, promoting droplet deformation and breakup, or

smaller droplets. Inversely, in image a), the dispersed phase ($_{HMW}$ PLLA) is more viscous and more elastic than the matrix ($_{HMW}$ PMLA) and $\kappa > 1$. The droplets exhibit a greater resistance to deformation and breakup is less efficient, favoring the formation of larger droplets [37], [62], [63], [64], [65].

However, phase images obtained at higher magnification in tapping mode at room temperature (Fig. 3) seem to suggest partial miscibility for blends of 30 wt% and 70 wt% $_{HMW}$ PLLA. Both phases appear to display to some degree heterogeneity due to the presence of inclusions of the minor phase in the major phase and vice versa, as can be clearly discerned in the phase images of Fig. 3. However, this heterogeneity could also result from crystallisation-induced phase separation. Bouapao *et al.* [47] found that the addition of PDLLA, an amorphous polylactide, to PLLA significantly affects the crystallisation kinetics. PDLLA is excluded from PLLA crystalline domains, slowing crystal growth and creating PDLLA amorphous region alongside crystalline PLLA ones. The presence of heterogeneity in the blends of 30 wt% and 70 wt% $_{HMW}$ PLLA is further corroborated and visualised in the AFM-IR images mapped at a wavenumber of 1750 cm^{-1} and shown in Fig. 4 and 5.

Contrast could also be achieved for the blend containing 90 wt% $_{HMW}$ PLLA, though less obvious than in other blends. The observed morphology in the latter consists of two distinct phases with small, darker in color, $_{HMW}$ PMLA dispersed droplets in the $_{HMW}$ PLLA matrix of lighter color. This phase separation becomes more obvious in Figure 3 d) where the high magnification phase image of the inset reveal heterogeneity within the small dispersed $_{HMW}$ PMLA phase consistent with partial miscibility, although the two phases remain largely distinct.

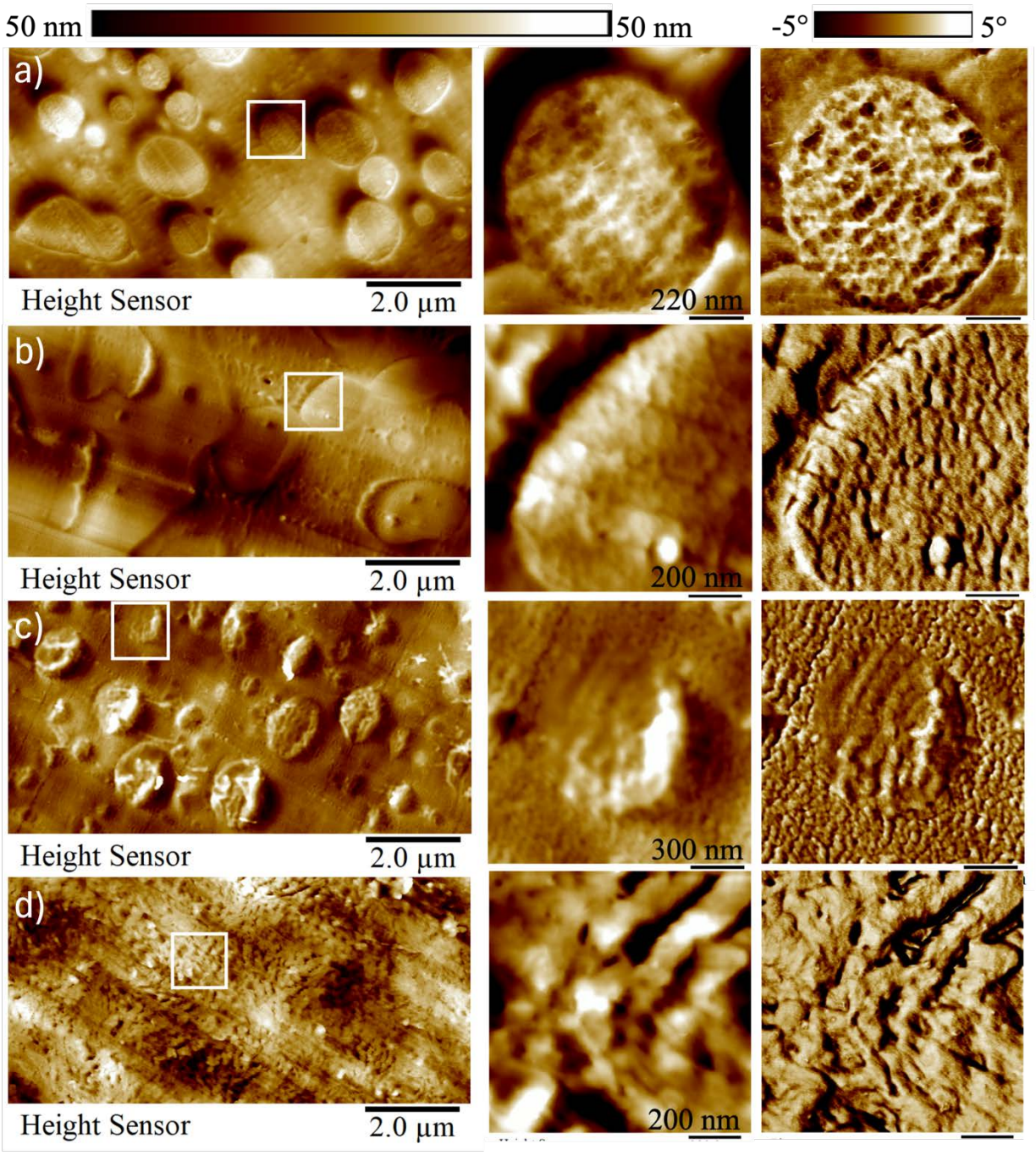

Figure 4.3 Tapping Mode AFM images of $_{HMW}$ PLLA/ $_{HMW}$ PMLA blends with (a) 30 wt% $_{HMW}$ PLLA (b) 50 wt% $_{HMW}$ PLLA (c) 70 wt% $_{HMW}$ PLLA and (d) 90 wt% $_{HMW}$ PLLA content. Left: 10µm × 5µm Height Sensor topographic image, center: topographic image of zoom inset & right: Phase image of zoom inset.

Additional phase composition was confirmed using Resonance Enhanced AFM-IR. The combination of AFM's high resolution and IR spectroscopy's compositional characterization capabilities enabled the spatial distribution of each polymer phase to be resolved at the nanometer scale, which was then correlated with their chemical identification and overcoming the diffraction limit of conventional infrared (IR) spectroscopy. With the help of AFM-IR, we were able to chemically distinguish the $_{HMW}$PMLA phase from the $_{HMW}$PLLA phase in $_{HMW}$PLLA/ $_{HMW}$PMLA blends containing a) 70 wt% $_{HMW}$PLLA and b) 30 wt% $_{HMW}$PLLA (Fig. 4). Figure 4 c) illustrates the AFM-IR spectra generated for the $_{HMW}$PLLA phase (blue) and the HMW PMLA phase (red). The positions at which the spectra were acquired are labelled on the topographic image in Figure 5 a) and b) as the blue and red cursors. Both spectra were very similar, with differences in the carbonyl stretching spectral region. The AFM-IR spectrum of $_{HMW}$PMLA (in red) reveals two broad, less defined carbonyl stretch bands at 1776 and 1750 cm^{-1}, while the more crystalline $_{HMW}$PLLA phase (in blue) shows splitting and narrowing of the carbonyl stretching modes, with the additional bands positioned at 1761 and 1780 cm^{-1}. The ester stretching spectral region is known to be sensitive to molecular order and conformation, as coupling of the C=O groups is expected for PLLA [66]. Such narrowing of bands has also been reported in the literature and has been linked to a highly ordered interlamellar state within a semicrystalline PLLA phase [67].

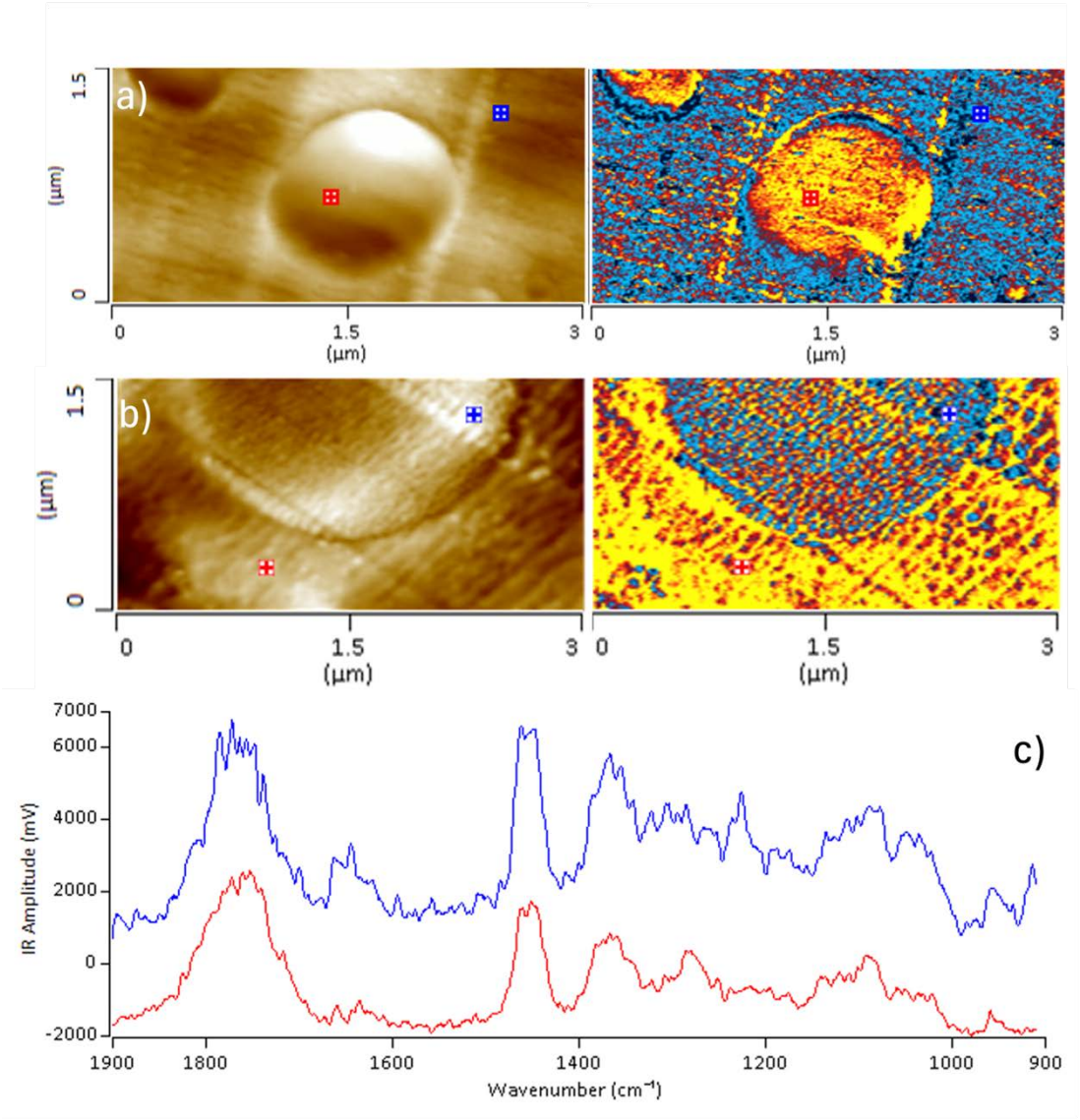

Figure 4.4 Morphological and compositional phase identification of two $_{HMW}$ PLLA/ $_{HMW}$ PMLA blends containing (a) 70 wt% HMW PLLA & (b) 30 wt% $_{HMW}$ PLLA , by photothermal AFM-IR. Left : 3µm × 1,5µm topographic AFM image & right: corresponding AFM-IR chemical map acquired at 1750 cm-1, highlighting the strong C=O stretch absorption of the $_{HMW}$ PMLA phase in yellow, (c) AFM-IR spectra for the $_{HMW}$ PMLA (red) and PLLA (blue).

IR mapping of the $_{HMW}$ PMLA phase was performed on both blends by irradiating the area directly beneath the scanning probe with IR excitation fixed at 1750 cm^{-1} throughout the scans. The AFM-IR maps presented in Figure 5 (a) and (b) clearly depict the strongly absorbing $_{HMW}$ PMLA phase

(in yellow) against the $_{HMW}$ PLLA phase (in blue). Figure 5 (a) shows the 70 wt% $_{HMW}$ PLLA blend, which displays an absorbing $_{HMW}$ PMLA droplet phase (in yellow) dispersed in a $_{HMW}$ PLLA matrix (in blue). Inversely, the 30 wt% $_{HMW}$ PLLA blend displays much smaller $_{HMW}$ PLLA droplet phase (in blue), dispersed in an absorbing $_{HMW}$ PMLA matrix (in yellow). Higher-magnification (3 µm × 1.5 µm) AFM-IR maps of both blends, performed at 1750 cm^{-1} (Fig. 4), also suggest heterogeneity of the two phases, with smaller, nanometer-sized absorbing domains appearing scattered throughout the blue phase and vice versa.

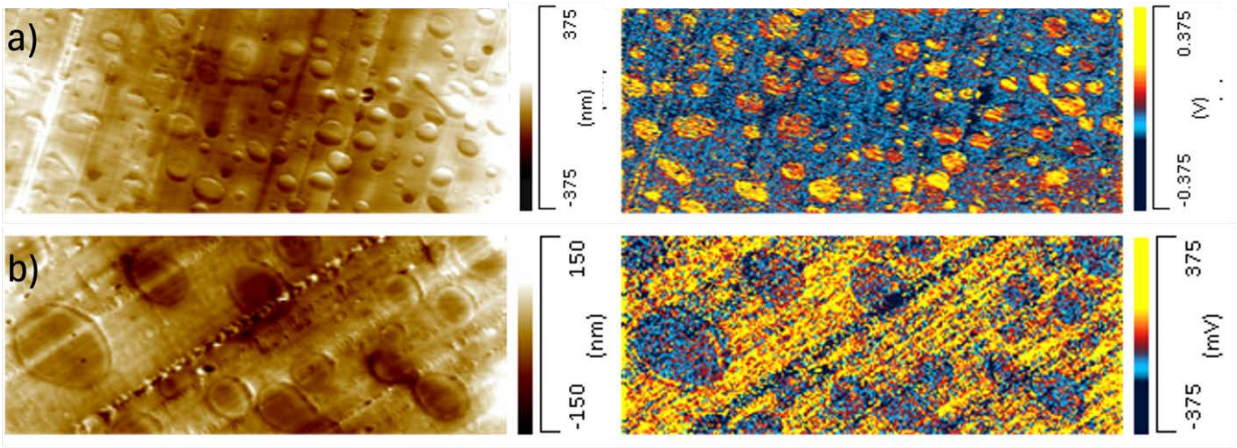

Figure 4.5 Morphological and compositional phase identification of two $_{HMW}$ PLLA/ $_{HMW}$ PMLA blends containing (a) 70 wt% $_{HMW}$ PLLA & (b) 30 wt% $_{HMW}$ PLLA by photothermal AFM-IR: Left : 25µm × 10µm topographic AFM image & right: corresponding AFM-IR chemical map at 1750 cm-1, highlighting the strong C=O stretch absorption of the $_{HMW}$ PMLA phase in yellow.

Table 4.2 Mean radius in number average R_n and in volume average R_v and polydispersity of the 30% and 70% $_{HMW}$ PLLA blend

Blend composition	Volume average R_v (µm)	Number average R_n (µm)	Polydispersity I
30 $_{HMW}$ PLLA / 70 $_{HMW}$ PMLA	1.50 ± 0.10	0.90 ± 0.10	1.72
70 $_{HMW}$ PLLA / 30 $_{HMW}$ PMLA	0.71 ± 0.02	0.36 ± 0.03	1.97

4.4.2 Thermal Analysis

The thermograms of all four different PLA are presented in Figure 6 and the DSC results are presented in Table III and IV. The experimental T_g of high and low molecular weight PLLA are 61.8 ± 0.4 °C and 61.5 ± 0.1 °C, while they are 48.2 ± 0.1 °C and 47.6 ± 0.1 °C for PMLA. $_{HMW}$ PMLA and $_{LMW}$ PMLA are completely amorphous while both PLLA are semi-crystalline. The melt transition temperature of $_{HMW}$ PLLA and $_{LMW}$ PLLA are 178.1 ± 0.4 °C and 177.6 ± 0.1 °C respectively, while their cold crystallisation temperature (T_{cc}) are 106.0 ± 0.4 °C and 105.1 ± 0.4 °C and their crystallisation temperature (T_c) are 103.1 ± 0.5 °C and 105.6 ± 0.4 °C. $_{HMW}$ PLLA and $_{LMW}$ PLLA have a crystallinity of 27 ± 1 % and 12 ± 1 % during the second heating, and of 1.4 ± 0.4 % and 2.6 ± 0.2 % during cooling. Pan *et al.* [24] observed that the T_g, the T_m and the T_{cc} of PLLA increase with molecular weight. They also reported that the crystallisation rate of PLLA during cooling increases as molecular weight decreases, which could promote a higher crystalline content. This can explain what is observed here.

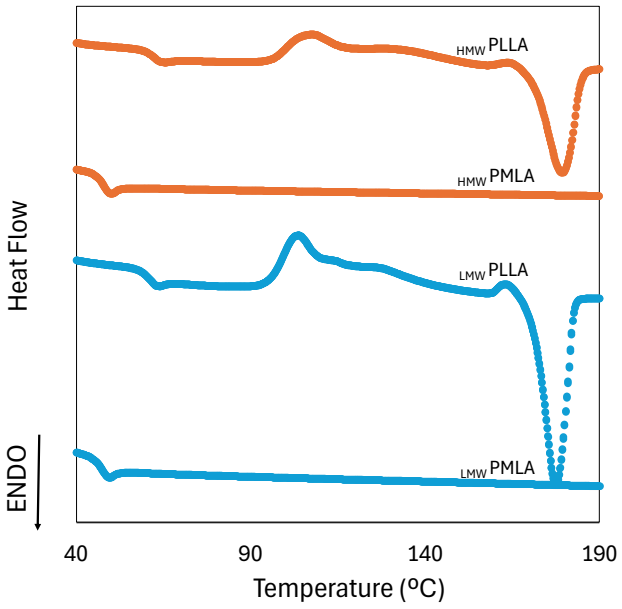

Figure 4.6 Thermograms of neat PLLA and PMLA of low and high molecular weight

Table 4.3 DSC results from second heath curve of PLLA and PMLA low and high molecular weight

Samples	T_g (°C)	T_m (°C)	ΔH_m(J/g)	T_{cc} (°C)	ΔH_{cc}(J/g)	X(%)
$_{HMW}$ PMLA	48.2 ± 0.1					
$_{LMW}$ PMLA	47.6 ± 0.1					
$_{HMW}$ PLLA	61.8 ± 0.4	178.1 ± 0.4	35.0 ± 1.0	106.0 ± 0.4	9.8 ± 0.7	27.0 ± 1.0
$_{LMW}$ PLLA	61.5 ± 0.1	177.6 ± 0.1	43.0 ± 0.8	105.1 ± 0.4	32.0± 0.6	12.0 ± 1.0

Table 4.4 DSC results from cooling of $_{HMW}$ PLLA and $_{LMW}$ PLLA

Samples	T_g (°C)	T_c (°C)	ΔH_c(J/g)	X(%)
$_{HMW}$ PLLA	59.1 ± 0.1	103.1 ± 0.5	1.3 ± 0.1	1.4 ± 0.4
$_{LMW}$ PLLA	59.2 ± 0.2	105.6 ± 0.4	2.4± 0.2	2.6 ± 0.2

The glass transition temperature (T_g) is a key indicator of a blend miscibility. The observation of a single T_g suggests the presence of a single homogeneous phase and, consequently, miscibility, while the presence of multiple glass transitions reveals multiple phases and therefore immiscibility [68], [69]. Partial miscibility can also be investigated through DSC. In binary blends, partial miscibility is typically reflected by the deviation of the blend's glass transitions from the glass transition of its neat components. If the T_g remains unchanged from the neat components, this reveals complete immiscibility [38]. Figure 7 presents the thermograms for all blends of $_{HMW}$ PLLA with $_{HMW}$ PMLA. As previously noted, the thermograms were shifted vertically for clarity.

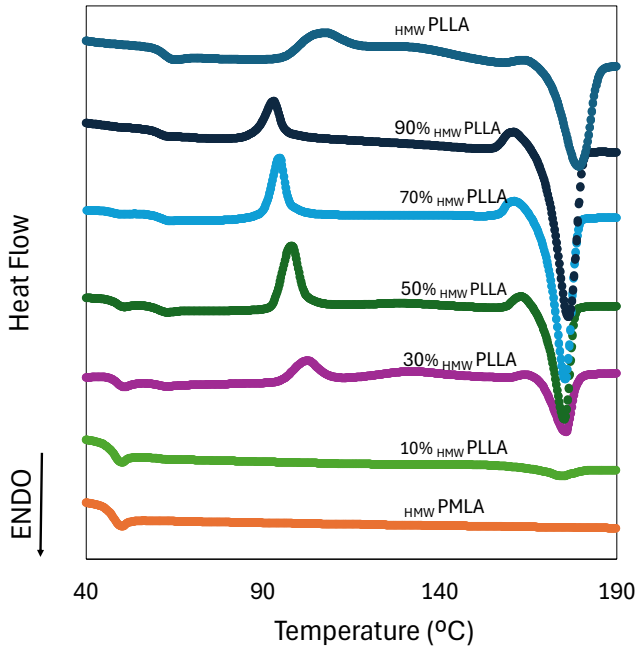

Figure 4.7 Thermograms of HMW PLLA and HMW PMLA blends

The Fox equation gives further information on miscibility. This equation relates the blend composition to the glass transition of the neat phases to determine the expected glass transition for a miscible system [68], [69].

$$\frac{1}{T_g} = \frac{w_1}{T_{g,1}} + \frac{w_2}{T_{g,2}} \tag{6}$$

Figure 8 shows the glass transition of all the high molecular weight PLLA and PMLA blends. The dotted line represents the glass transitions predicted by the Fox equation, indicating miscibility at this composition. The presented T_g 1 and T_g 2 are the glass transition temperature associated with the HMW PMLA and the HMW PLLA phases, respectively. The blends with a composition of 30 wt% HMW PLLA, 50 wt% HMW PLLA and 70 wt% HMW PLLA all show distinctly two glass transitions with little to no deviation from the neat phases. These results indicate immiscibility for all these blend compositions, as indicated by the morphology observed via AFM. Bouapao *et al.* [47] also reported the presence of two distinct T_g for PLLA and poly(DL-lactide) PDLLA blends containing 70, 50, 40 and 30 wt% PLLA. PDLLA is an amorphous PLA synthesized from L-Lactide and D-

Lactide, while PMLA is synthesized from meso-Lactide. They therefore also concluded immiscibility of the blends at these compositions.

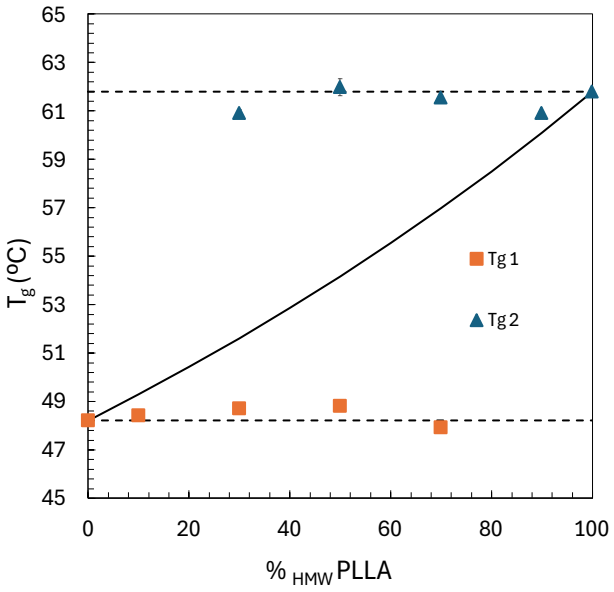

Figure 4.8 Glass transition temperatures of HMW PLLA and HMW PMLA blends

The blends of 10 wt% HMW PLLA and 90 wt% HMW PLLA present a single T_g associated with the matrix phase. The single T_g of both blends show a slight deviation from the neat polymer. However, the shift remains within the instrumental uncertainty and cannot be considered significant. The presence of a second glass transition is unclear. Given the proximity of the T_g values of HMW PLLA and HMW PMLA and the low contribution of the dispersed phase, any secondary transition is likely below the detection limit of the instrument. The system therefore does not appear fully miscible, although this conclusion is limited by experimental resolution. Bouapao *et al.* [47] also observed a single T_g for blends containing 10 and 90 wt% PLLA under quenched conditions. The 90 wt% HMW PLLA blend exhibited two T_g values when not quenched.

4.4.3 Rheological Analysis

The SAOS data of the four different PLAs and their blends are presented in Figure 9. The neat PMLA exhibits a lower complex viscosity than the neat PLLA, regardless of the molecular weight, which can be attributed to the disrupted stereochemistry of PMLA, or its greater flexibility [17].

Furthermore, the higher molecular weight PLAs show increased viscosity, as seen experimentally by Yang *et al.* [36], and as expected by their longer chain lengths. All neat polymers present a nearly linear viscoelastic behavior with a long terminal zone, with a long plateau for the complex viscosity and a slope of approximately 2 for the storage modulus at lower frequency on the log-log scales [35].

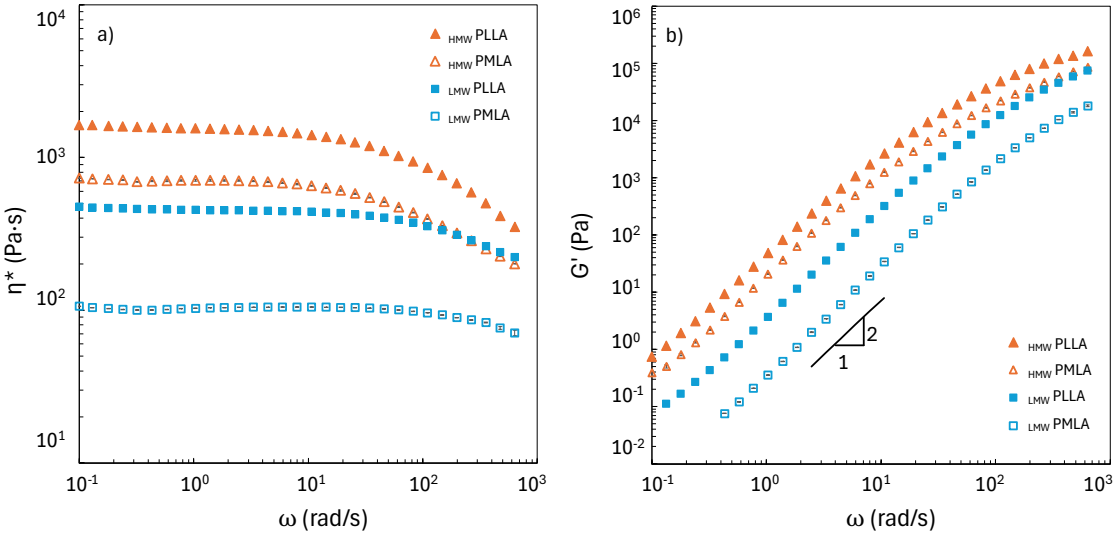

Figure 4.9 Complex viscosity (a) and storage modulus (b) of the neat PLLA and PMLA at 190 °C

Figure 10 presents the SAOS results for all blend compositions of the high molecular weight $_{HMW}$ PLLA and $_{HMW}$ PMLA. All blends deviate from the slope of 2 and exhibit a shoulder at lower frequencies, which gradually decreases from 0.1 rad/s to lower frequencies. This behavior is the result of the contribution of interfacial tension, precisely of the relaxation of the droplets of the dispersed phase for emulsion type morphology and of the relaxation of the continuous network for a co-continuous morphology [6], [70], [71], [72], [73]. The interfacial contribution is particularly pronounced for blends with compositions of 30/70, 50/50 and 70/30 wt/wt% of $_{HMW}$ PLLA/ $_{HMW}$ PMLA, suggesting immiscibility for these compositions.

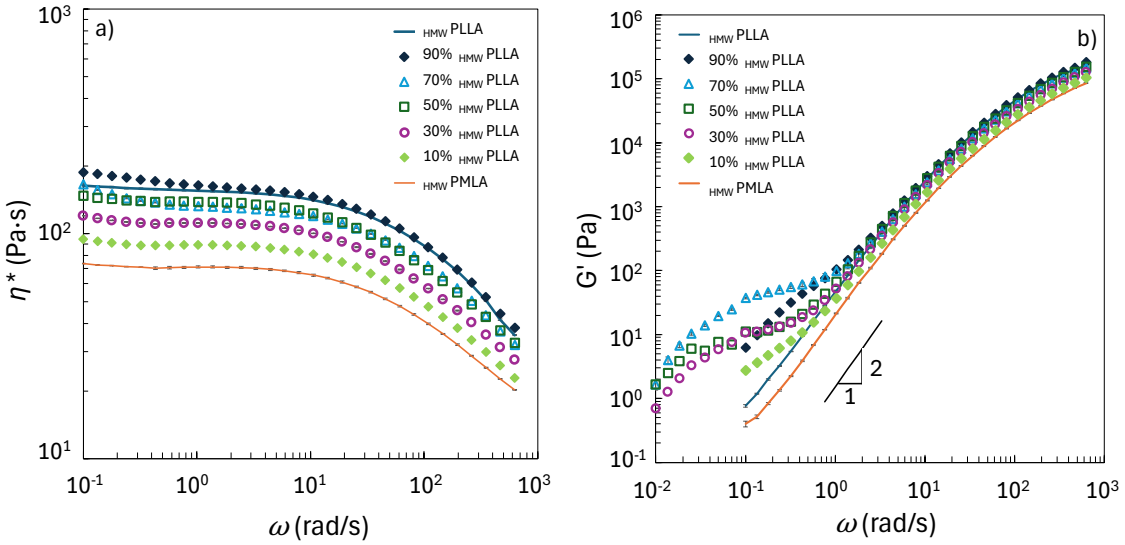

Figure 4.10 Complex viscosity (a) and storage modulus (b) of $_{HMW}$ PLLA and $_{HMW}$ PMLA blends at 190 °C

The 90% $_{HMW}$ PLLA blend shows higher viscosity values than the neat $_{HMW}$ PLLA at low frequencies, which could be attributed to the morphology observed by AFM, specifically the presence of the smaller dispersed phase for this composition. For the 10% and 90% $_{HMW}$ PLLA blends, the shoulder is less pronounced, and no visible decrease is observed. No reliable data could be acquired for angular frequency lower than 0.1 rad/s as the modulus approached the sensitivity limit of the rheometer. The slight shoulder observed in the storage modulus could be explained by immiscibility, the reduced interfacial contribution due to the smaller volume fraction of the dispersed phase. This deviation could also be the result of partial miscibility, as phase separation translates in an increase in *G'* in the terminal zone [11]. These behaviors are also present in blends of low molecular weight blends PLLA and PMLA as well as high with low molecular weight blends PLLA or PMLA (see the supplementary material, Fig. S1, S2 and S3).

Rheological models are great tools to predict the behavior of polymer blends and estimate the interfacial tension between their components. They can also provide insights on the miscibility or immiscibility of the components. The Palierne model is a well-established model to predict the linear viscoelastic behavior of an immiscible polymer blend of an emulsion type morphology with spherical dispersed droplets of nearly uniformed size. This model is valid for a droplet size

polydispersity smaller than 2 while droplet interactions, such as breakup and coalescence, are not considered [6], [70], [71], [72], [73]. The Palierne model can be expressed as:

$$G_B^*(\omega) = \frac{1 + 3\sum_i \phi_i H_i^*(\omega)}{1 - 2\sum_i \phi_i H_i^*(\omega)} G_M^*(\omega) \tag{7}$$

where

$$H_i^*(\omega) = \frac{4\left(\frac{\alpha}{R_v}\right)[2G_m^*(\omega) + 5G_d^*(\omega)] + [G_d^*(\omega) - G_m^*(\omega)][16G_m^*(\omega) + 19G_d^*(\omega)]}{40\left(\frac{\alpha}{R_v}\right)[G_m^*(\omega) + G_d^*(\omega)] + [2G_d^*(\omega) + 3G_m^*(\omega)][16G_m^*(\omega) + 19G_d^*(\omega)]} \tag{8}$$

ϕ is the volume fraction of the dispersed phase, R_v is the average radius in volume of the dispersed droplets, α the interfacial tension, $G_B^*(\omega)$, $G_m^*(\omega)$ and $G_d^*(\omega)$ the complex modulus of the blend, the matrix and the dispersed phase respectively. The parameter α, the interfacial tension of the blend components, was fitted by minimising the mean square error between the storage moduli estimated by the Palierne model and the experimental SAOS data of the $_{HMW}$PMLA/ $_{HMW}$PLLA blend over the lower frequencies. The blend of 50% was not estimated, as the morphology is co-continuous.

The Palierne model fits for the blends of 10 wt% $_{HMW}$PLLA, 30 wt% $_{HMW}$PLLA, 70 wt% $_{HMW}$PLLA and 90 wt% $_{HMW}$PLLA are shown as solid lines in Figure 11. The data for the 30 wt% $_{HMW}$PLLA and 70 wt% $_{HMW}$PLLA blends are fairly well described by the model. However, the agreement is not perfect, which could be the result of the heterogeneity observed in both phases via AFM. This close agreement between the experimental data and the fits confirms the validity of the Palierne model assumptions. The interfacial tension estimated with the model is presented in Table V. Both compositions present comparable interfacial tension values, 0.15 mN/m ± 0.02 and 0.10 mN/m ± 0.03. These values are relatively low compared to other PLA-containing blends, such as PLA/PBAT 1.25 mN/m and PLA/PBSA 1.57 mN/m, estimated by Nofar *et al.* [71] using Palierne fitting. A relatively low interfacial tension is expected for $_{HMW}$PLLA/ $_{HMW}$PMLA blend, as both phases are PLA-based.

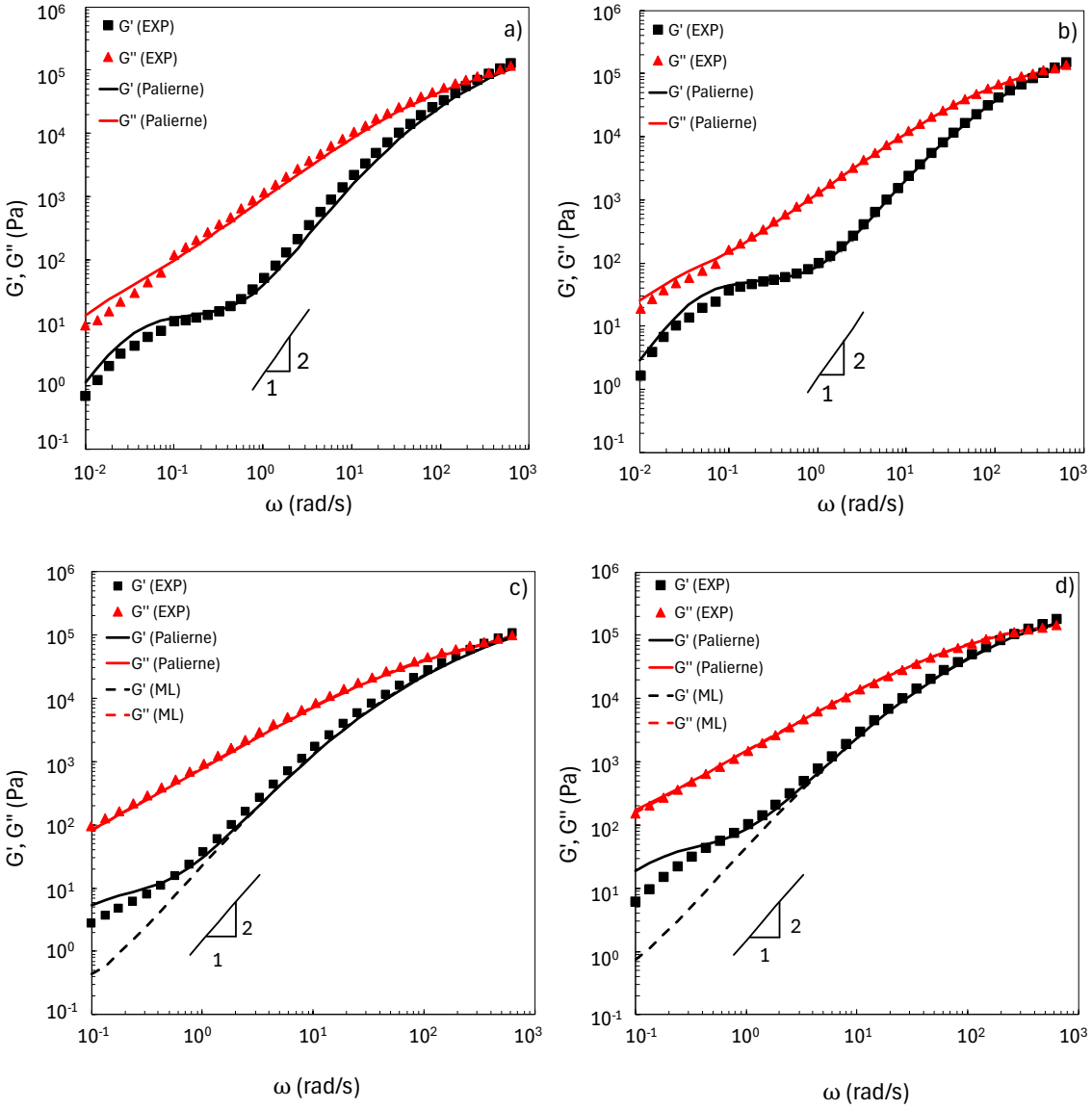

Figure 4.11 Loss and storage moduli of the blends of high molecular weight PLLA and PMLA of (a)30 wt% $_{HMW}$ PLLA (b) 70 wt% $_{HMW}$ PLLA (c) 10 wt% $_{HMW}$ PLLA and (d) 90 wt% $_{HMW}$ PLLA content at 190 °C fitted with the Palierne model (Palierne) and the mixing law (ML)

Table 4.5 Interfacial Tension obtained from the Palierne model of the 30% and 70% $_{HMW}$ PLLA blend

% of $_{HMW}$ PLLA in the blend	Interfacial Tension α (mN/m)	Radius *Rv* (μm) (from Table 2)
30	0.15 ± 0.02	1.50 ± 0.10
70	0.10 ± 0.03	0.71 ± 0.02

The model for the 10 wt% $_{HMW}$ PLLA and 90 wt% $_{HMW}$ PLLA overpredicts the interfacial contribution at lower frequencies. This could imply that these blend components are not fully immiscible, as previously stated. The SAOS data of these two blends were also fitted with the mixing law (dashed lines in Figure 11 c and d), a model that can predict the viscosity of miscible systems [7] :

$$\log \eta_b = w_d \log \eta_d + (1 - w_d) \log \eta_m \quad (9)$$

where w_d is the weight fraction of the dispersed phase, η_b , η_d and η_m are the viscosity of the blend, the dispersed phase and the matrix respectively.

At low frequencies, the model underestimates the storage modulus of the blend; there is therefore a contribution of interfacial tension, and these blend components are not fully miscible. Partial miscibility is then again suspected here because of the presence of this shoulder as well as the deviation of the mixing law at lower frequencies [8].

A temperature sweep could provide insights on the degree of miscibility at these compositions, as changes in temperature would modify the system's position within the phase. However, temperature-dependent rheological measurements in the melt are not easily carried out for PLA-based systems. Sperenza et al. reported a progressive decrease in the Newtonian plateau of the complex viscosity of dried neat PLLA over time, with the onset occurring much earlier at 220 °C (around 1000 s) than at 180 °C (around 10 000 s) [74]. Thermal [26] and shear stresses[27] arising

from both blend processing and frequency sweep measurement further accelerate PLA degradation, thereby limiting the maximum temperature for rheological measurements. The relatively high melting temperature of PLLA also restricts the accessible temperature window. Another approach could be to investigate the miscibility at lower contents of the dispersed phase. However, the low modulus values obtained at low frequencies approach the sensitivity limits of conventional rheometers. Moreover, obtaining low frequency rheological data requires long measurement times, which further degrades PLA. These constraints limit the applicability of melt rheology for probing miscibility for this system and obtaining phase diagrams.

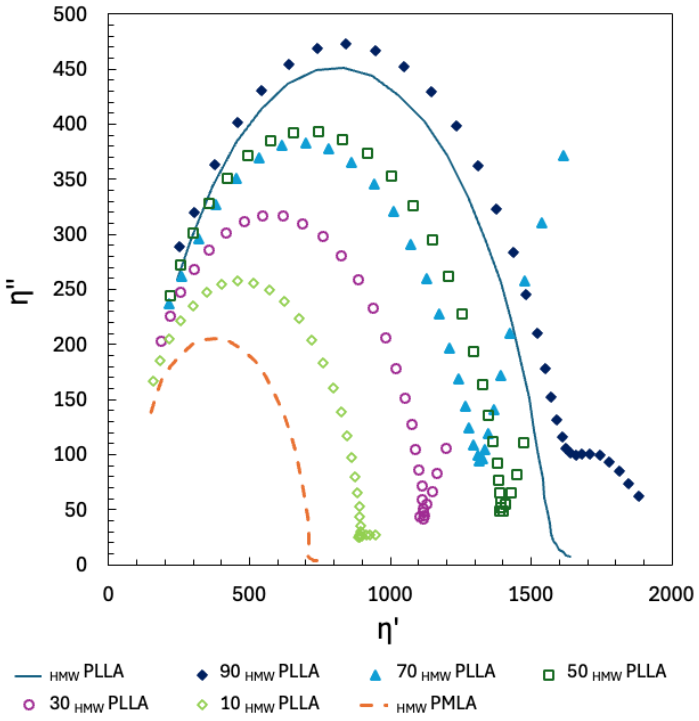

Figure 4.12 Cole-Cole plots of $_{HMW}$ PLLA and $_{HMW}$ PMLA blends at 190°C

Determining the relaxation times is another powerful tool to evaluate the miscibility of blends. Cole-Cole plots of the different blends of high molecular weight $_{HMW}$ PMLA and $_{HMW}$ PLLA were also obtained and are presented in Figure 12. The imaginary part of the complex viscosity η'' is plotted against the dynamic viscosity η', illustrating the different relaxation modes of the blends. The neat polymers present a single arc, which represents a single relaxation mode, therefore a single phase. The blends of 30 wt% $_{HMW}$ PLLA, 50 wt% $_{HMW}$ PLLA and 70 wt% $_{HMW}$ PLLA presents

an arc followed by a rise, corresponding to two different relaxation modes, therefore indicative of immiscibility of the polymer components. The blends with 10 wt% $_{HMW}$ PLLA and 90 wt% $_{HMW}$ PLLA exhibits miscibility, since a single arc is visible. These results seem to contradict the previous conclusions of partial miscibility. However, the interfacial tension contribution is small and limited data were acquired at low frequencies. This likely prevents the full observation of the second relaxation mode.

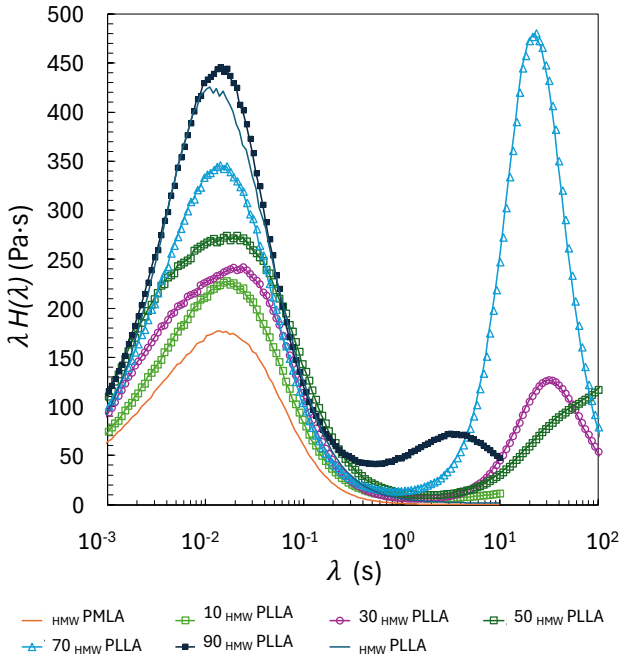

Figure 4.13 Weighted relaxation spectra of $_{HMW}$ PLLA and $_{HMW}$ PMLA blends at 190°C

If we relate these Cole-Cole plots to the relaxation spectra obtained from the SAOS data and calculated by NLREG and presented in Figure 13, we can observe these different relaxation modes. The relaxation times are indicated in Table VI. For the neat polymers, we see a single relaxation mode, with a characteristic time of 0.011 s for the $_{HMW}$ PLLA and at 0.014 s for the $_{HMW}$ PMLA. These are indicative of the PLA nature and correspond to the backbone relaxation of PLA chains. The typical relaxation time reported for PLA is around 0.01 s [9], [75]. The relaxation peak of $_{HMW}$ PMLA exhibits a lower amplitude than that of $_{HMW}$ PLLA, or a smaller contribution to the relaxation mechanism. The area under the curve of the relaxation spectra corresponds to the zero-shear viscosity η_0 [76], implying that $_{HMW}$ PLLA's viscosity is higher than $_{HMW}$ PMLA, as experimentally observed. Randall *et al.* [17] reported a smaller block length and characteristic ratio

for PMLA compared to PLLA, supporting the enhanced chain mobility that could contribute to this behavior.

For the immiscible blends containing 30 and 70 wt% $_{HMW}$ PLLA, a second relaxation time is observed. This relaxation is associated with the relaxation of the droplets of the dispersed phase within the matrix and reflects the contribution of interfacial tension. In other words, the relaxation time λ_2 represents the time required for a droplet to recover its equilibrium spherical shape. The blend of 50% wt% $_{HMW}$ PLLA presents a shoulder rather than a distinct peak, which extends to latter relaxation time, not reached in the range of frequency tested. This behavior can be attributed to the co-continuous morphology of this blend [77]. The amplitude difference between the different compositions can be explained by the viscosity ratio. During rheological measurements, droplets of the dispersed phase are deformed and they store energy. More energy is stored for more easily deformable droplets, which corresponds to the case of a small viscosity ratio [78]. Since the $_{HMW}$ PMLA has a lower viscosity than the $_{HMW}$ PLLA, the viscosity ratio is smaller when the $_{HMW}$ PMLA is the dispersed phase and the $_{HMW}$ PLLA is the matrix. The amplitude observed in the relaxation spectra peaks is therefore more important as more energy is stored. This would explain why the 70 wt% $_{HMW}$ PLLA blend has a higher amplitude than the 30 wt% $_{HMW}$ PLLA blend.

The blends containing 10 wt% and 90 wt% $_{HMW}$ PLLA also exhibit a second relaxation process in Figure 13, although less pronounced than the fully immiscible blends. This relaxation can also be attributed to the contribution of interfacial tension. For the 10 wt% $_{HMW}$ PLLA blend, there is as a slight increase in the relaxation spectrum, indicating a small interfacial contribution. In the 90 wt% $_{HMW}$ PLLA blend, the contribution is more pronounced and comparable in amplitude to the contribution in the 30 wt% $_{HMW}$ PLLA blend. This is consistent with the low viscosity ratio in this composition, which favors stronger droplet deformation and higher stored elastic energy, therefore a higher amplitude [78]. Moreover, the second relaxation times observed for the 10 wt% $_{HMW}$ PLLA and 90 wt% $_{HMW}$ PLLA blends occur at shorter times than those of the fully immiscible blends. This shift toward shorter relaxation times implies that the dispersed phase of these blends relaxes more rapidly, which could be explain with the assumption of partial miscibility.

The relaxation time λ_2 associated with the contribution of interfacial tension can also be predicted by the Palierne model with Equation 10 [79].

$$\lambda_2 = \frac{R_v \eta_m}{4\alpha} \frac{(19\kappa + 16)\,[2\kappa + 3 - 2\phi(\kappa - 1)]}{10(\kappa + 1) - 2\phi(5\kappa + 2)} \tag{10}$$

where κ is the viscosity ratio.

The relaxation time λ_2 was estimated for the blends of 30 wt% $_{HMW}$ PLLA and 70 wt% $_{HMW}$ PLLA only, as these are the compositions for which Palierne model provides reliable predictions. They are presented in Table VI alongside the relaxation times obtain from the relaxation spectra. The relaxation times obtained from the Palierne model are consistent with those observed from the NLREG calculated relaxation spectra, indicating good agreement with Palierne and further reinforcing the conclusion that these blends are completely immiscible.

Table 4.6 Relaxation times obtained from the relaxation spectra and from the Palierne equation for the $_{HMW}$ PLLA and $_{HMW}$ PMLA blends

$_{HMW}$ PLLA Content (%)	Relaxation Time λ_1 (s)	Relaxation Time λ_2 (s)	Relaxation Time Estimated by the Palierne model λ_2(s)
0	0.014	-	-
10	0.017	unreached	-
30	0.024	31	30
50	0.021	unreached	-
70	0.014	23	23
90	0.014	3.1	-
100	0.011	-	-

4.5 Conclusion

In this study, the morphology, thermal and rheological properties of poly(meso-lactide) (PMLA) blended with poly(L-lactide) (PLLA) were determined for a wide range of compositions and different molecular weights. PMLA, an amorphous polylactide, has a lower glass transition than PLLA and present no crystallinity. In addition, PMLA also displays a lower viscosity as well as storage and loss moduli than PLLA, regardless of molecular weight. This behavior can be explained by the increased chain flexibility of the PMLA due to the highly disrupted stereo sequence of the backbone.

The PLLA and PMLA miscibility was investigated through DSC, AFM and SAOS measurements combined with model fitting. The blends presented immiscibility at compositions of 30/70, 50/50 and 70/30 wt/wt% of $_{HMW}$ PLLA/ $_{HMW}$ PMLA. DSC analysis revealed two distinct glass transition temperatures corresponding to $_{HMW}$ PLLA and $_{HMW}$ PMLA without any detectable deviation with respect to the neat components, 48.2 ± 0.1°C and 61.8 ± 0.4 °C respectively. SAOS measurements revealed the presence of a shoulder at lower angular frequencies, which was successfully fitted with the Palierne model, an immiscible emulsion type model, for the blend of 30 wt% $_{HMW}$ PLLA and 70 wt% $_{HMW}$ PLLA. Analysis using Cole-Cole plots and NLREG-derived relaxation spectra identified two unique relaxation times: one linked to the intrinsic molecular behavior of PLA and another associated with the blend's interfacial dynamics. High-resolution AFM imaging verified that all immiscible blend compositions underwent phase separation, revealing an emulsion-type morphology in the 30 wt% and 70 wt% PLLA samples, while the 50 wt% PLLA blend exhibited a co-continuous architecture. Furthermore, nanomechanical mapping indicated structural heterogeneity within both phases of the 30 wt% and 70 wt% PLLA blends, a finding that was chemically validated through AFM-IR.

The blends with the compositions of 10 wt% $_{HMW}$ PLLA and 90 wt% $_{HMW}$ PLLA could be partly miscible. DSC analysis revealed a single glass temperature for both blends. However, SAOS results showed a small shoulder in the storage modulus at low frequencies that could not be fitted with either miscible nor immiscible models. In addition, a relaxation time associated with interfacial tension was identified for both compositions. The partial immiscibility in the blend of 90 wt% $_{HMW}$

PLLA was further corroborated by the presence of tiny droplets in the morphology images obtain by AFM, as well as the presence of heterogeneity in both phases.

The study demonstrates that the $_{HMW}$ PLLA/PMLA blend system exhibits composition-dependent behavior, transitioning from potential partial miscibility at extreme concentration ratios to distinct immiscibility at intermediate levels. Although PLLA and PMLA are chemically identical stereoisomers of the same PLA molecule, their different stereochemistry results in distinctly diverging properties: crystalline, isotactic PLLA versus amorphous, atactic PMLA. Despite their immiscibility, the shared polylactide backbone ensures relatively low interfacial tension between the phases.

We established a link between the thermal transitions, the rheological behavior and the specific emulsion-type and co-continuous morphologies identified by AFM's nanomechanical mapping. This provides a comprehensive understanding of how stereochemical differences dictate the functionality of PLLA/PMLA blends. Atomic force microscopy (AFM) has been a prevailing technique for acquiring nanomechanical, chemical, and structural properties of the blends, as it provided direct nanoscale visualisation of the dispersed states within the PLA blends and unraveled the complexity of their multilevel phase structure. Combining AFM's nanoscale investigation with statistically averaged critical macroscopic properties provided by DSC and SAOS rheology was instrumental in achieving a comprehensive understanding of the blends. This approach is essential for designing novel materials, as it successfully bridges the gap between the intricate molecular architecture of the blends and their macroscopic behaviour and, ultimately, their performance.

Our findings show that strategically incorporating poly(meso-lactide) (PMLA) effectively tunes the rheological and mechanical performance of poly(L-lactide) (PLLA) blends. This is achieved by leveraging PMLA's flexible chain architecture to regulate chain mobility as well as accelerating biodegradation rates.

Supplementary Material

See the Supplementary Material for the graphics of the complex viscosity and storage modulus of $_{HMW}$ PLLA and $_{LMW}$ PMLA blends, $_{LMW}$ PLLA and $_{HMW}$ PMLA blends and $_{LMW}$ PLLA and $_{LMW}$ PMLA blends.

Acknowledgments

The authors would like to thank NatureWorks for providing the PLA samples and for technical insights from Marc Flodquist, Joseph Schroeder, James R. Valentine, and Osei Owusu. We also sincerely thank Matthieu Gauthier and Claire Cerclé for their valuable technical assistance with the experiments. Furthermore, the authors would like to acknowledge the Laboratoire de caractérisation des matériaux - LCM at Université de Montréal for providing access to the state-of-the-art SPM facility and expertise. This research was supported by Natural Sciences and Engineering Research Council of Canada (NSERC) Discovery Grants.

Author Declarations

Conflict of interests

The authors declare no conflict of interest.

Data Availability

The data that support the findings of this study are available from the corresponding author upon reasonable request.

CHAPTER 5 ADDITIONNAL RESULTS

5.1 Thermal Analysis

5.1.1 Differential Scanning Calorimetry

Differential Scanning Calorimetry was performed for all blends and neat polymers. Only the results of the high molecular weight PLLA and PMLA blends were presented in the article, but all blends were tested experimentally. Table 5.1 presents the results of the $_{HMW}$PLLA and $_{HMW}$PMLA blends, table 5.2 presents the results of the $_{LMW}$PLLA and $_{HMW}$PMLA blends, table 5.3 the results of the $_{LMW}$PLLA and $_{HMW}$PMLA blends and table 5.4 the results of the $_{LMW}$PLLA and $_{LMW}$PMLA blends.

Table 5.1 DSC results of blends of $_{HMW}$PLLA and $_{HMW}$PMLA

Blend Composition	T_{g1} (°C)	T_{g2} (°C)	T_m (°C)	T_{cc} (°C)	X (%)
30% $_{HMW}$PLLA 70% $_{HMW}$PMLA	48.6	52.7 ± 0.40	175.69 ± 0.02		4.2 ± 0.10
50% $_{HMW}$PMLA 50% $_{HMW}$PMLA	48.79 ± 0.05	62.0 ± 0.40	175.36 ± 0.06	97.82 ± 0.06	7.35 ± 0.05
70% $_{HMW}$PMLA 30% $_{HMW}$PMLA	47.91 ± 0.04	61.54 ± 0.02	183.2 ± 0.20	97.82 ± 0.06	20.7 ± 0.40

Table 5.2 DSC results of blends of $_{LMW}$ PLLA and $_{HMW}$ PMLA

Blend Composition	T_{g1} (°C)	T_{g2} (°C)	T_m (°C)	T_{cc} (°C)	X (%)
30% $_{LMW}$ PLLA 70% $_{HMW}$ PMLA	48.45 ± 0.09	60.53 ± 0.03	175.65 ± 0.02	123.2 ± 0.40	11.2 ± 0.90
50% $_{LMW}$ PLLA 50% $_{HMW}$ PMLA	48.9 ± 0.20	60.6 ± 0.20	175.8 ± 0.20	123.2 ± 0.20	10.8 ± 0.10

Table 5.3 DSC results of blends of $_{HMW}$ PLLA and $_{LMW}$ PMLA

Blend Composition	T_{g1} (°C)	T_{g2} (°C)	T_m (°C)	T_{cc} (°C)	X (%)
50% $_{HMW}$ PLLA 50% $_{LMW}$ PMLA	48.2 ± 0.10	60.04 ± 0.01	175.5 ± 0.20	99.5 ± 0.50	6.2 ± 0.20

Table 5.4 DSC results of blends of $_{LMW}$ PLLA and $_{LMW}$ PMLA

Blend Composition	T_{g1} (°C)	T_{g2} (°C)	T_m (°C)	T_{cc} (°C)	X (%)
50% $_{LMW}$ PLLA 50% $_{LMW}$ PMLA	47.7 ± 0.10	60.00 ± 0.04	175.2 ± 0.40	97.9 ± 0.2	13.4 ± 0.40

All the blends exhibit two distinct glass transitions for the compositions tested, 30, 50 and 70 wt% PLLA. This further confirms immiscibility at these compositions, as found in the high molecular blends, indicative that immiscibility of PLLA and PMLA is present for different molecular weights.

5.1.2 Dynamic Mechanical Analysis

Dynamic Mechanical Analysis (DMA) was not performed due to difficulties encountered during sample demolding. Because PLA is relatively brittle, the use of a release agent in the mold did not prevent fracture during unmolding, and several specimens broke upon removal. Attempts to use a PTFE sheet to facilitate demolding were also unsuccessful, as slight deformation of the samples occurred. Since DMA measurements are conducted in the solid state and require specimens with precise and well-defined geometry, these deformations rendered the samples unsuitable for reliable analysis.

5.2 Rheology

The temperature selected for the rheological measurements was first determined by DSC analysis. A temperature of 190 °C was chosen, as the melting transition of high-molecular-weight PLLA ends at 187 °C, ensuring that all samples were fully molten during rheological characterization.

5.2.1 Steady Shear Measurements

Rheological experiments were first performed in steady shear. In figure 5.1, the steady state and the complex viscosity were plotted against the shear rate/angular frequency for the $_{HMW}$ PLLA, the $_{HMW}$ PMLA and the $_{LMW}$ PLLA. The concordance between both acquired viscosities confirms that the Cox Merz rule, presented in Equation 5.1, is valid for all three tested neat PLA, as is observed in literature for PLA. Indeed, The Cox Merz rule is valid for linear PLA for a large range of shear rates and frequencies [35]. The validity of the rule implies that the data acquired in SAOS is valid under steady state [3].

$$\eta^*(\omega) = \eta(\dot{\gamma}) \tag{5.1}$$

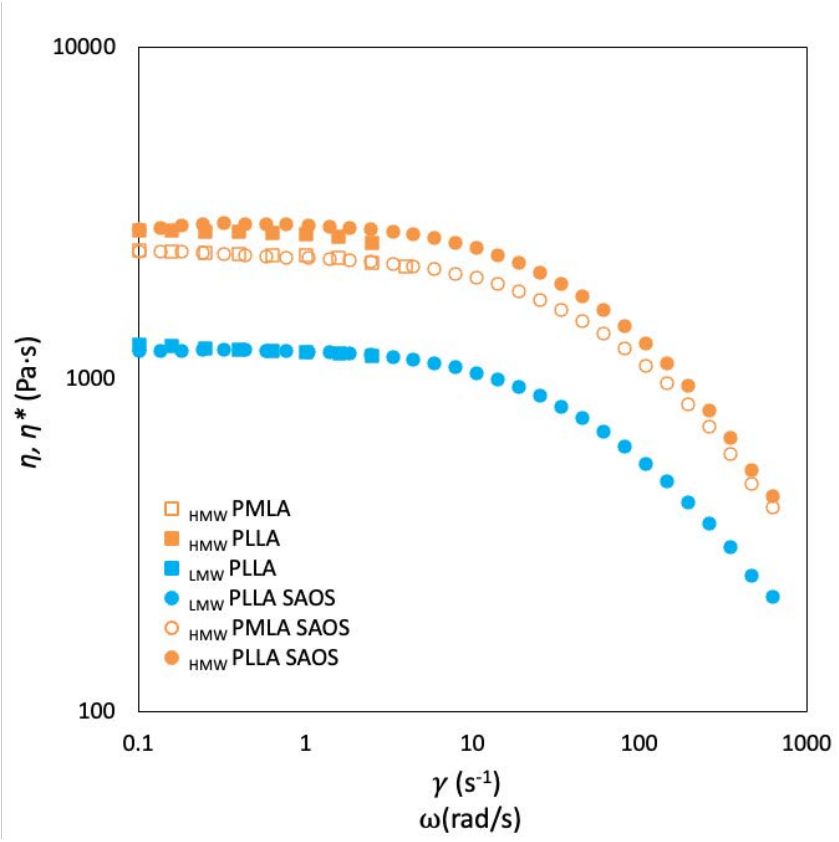

Figure 5.1 Complex and steady shear viscosity of $_{HMW}$ PLLA, $_{HMW}$ PMLA and $_{LMW}$ PLLA

5.2.2 Small-Amplitude Oscillatory Shear Measurements

The main rheological data were acquired in Small-Amplitude Oscillatory Shear (SAOS) mode. Prior to performing SAOS measurements, preliminary tests were conducted to ensure experimental conditions where within the linear viscoelastic (LVE) region. Both time sweep and amplitude sweep experiments were carried out to verify material stability and to identify the strain amplitude corresponding to the LVE domain.

An example of amplitude sweep is presented in Figure 5.2. High and low frequency were tested on multiple shear strain. Results concluded that a shear strain of 0.1, or 10%, was a good option for measurements, as no complex viscosity data went down, but the strain was also high enough to have good data resolution.

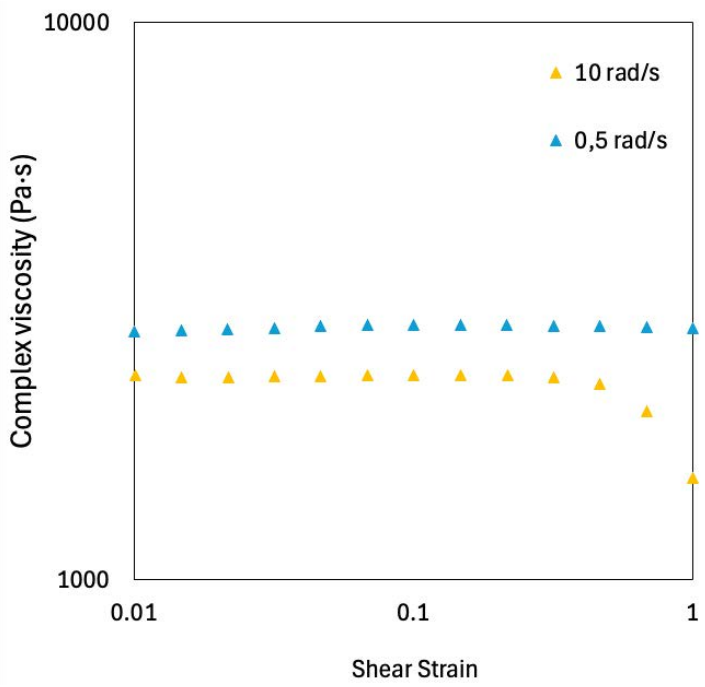

Figure 5.2 Complex viscosity of $_{HMW}$ PLLA obtain from amplitude sweep at 190 °C

Time sweep experiments were also performed, at an angular frequency of 10 rad/s and a strain amplitude of 10%. These measurements were carried out to evaluate the stability in time of the samples and to determine the time window over which the rheological data remain reliable. Figure 5.3 presents an example of time sweep for $_{HMW}$ PLLA and $_{HMW}$ PMLA.

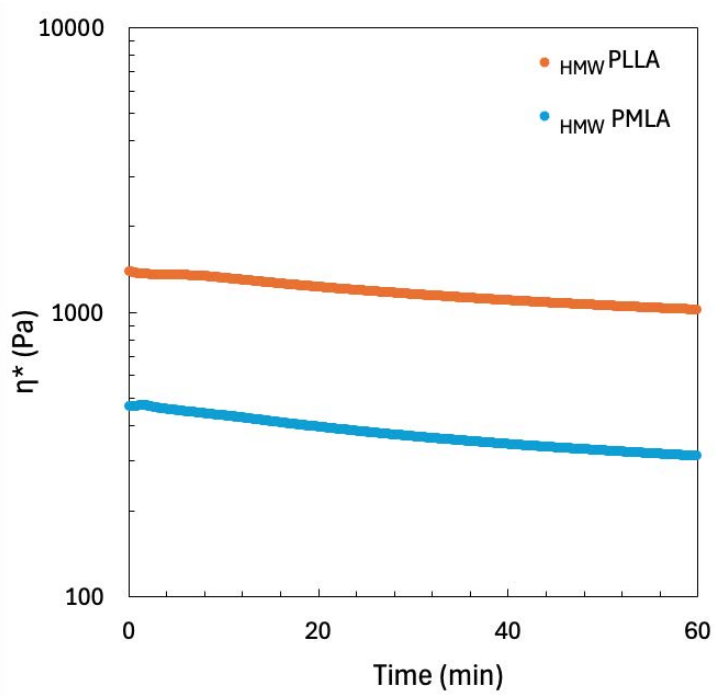

Figure 5.3 Complex viscosity of $_{HMW}$ PLLA and $_{HMW}$ PMLA obtained from time sweep at 190 °C

Only high molecular weight PLLA and PMLA blends rheology results were presented in the article. However, SAOS measurements were realised for all blends of PMLA and PLLA. Figures 5.4, 5.5 and 5.6 present the results of these blends. The beginning of the shoulder in the storage modulus at low frequency is visible for all blends. This shoulder is the clear sign of interfacial contribution, therefore confirming immiscibility for the compositions of 30, 50 and 70 wt% PLLA of all blends, low or high molecular weight.

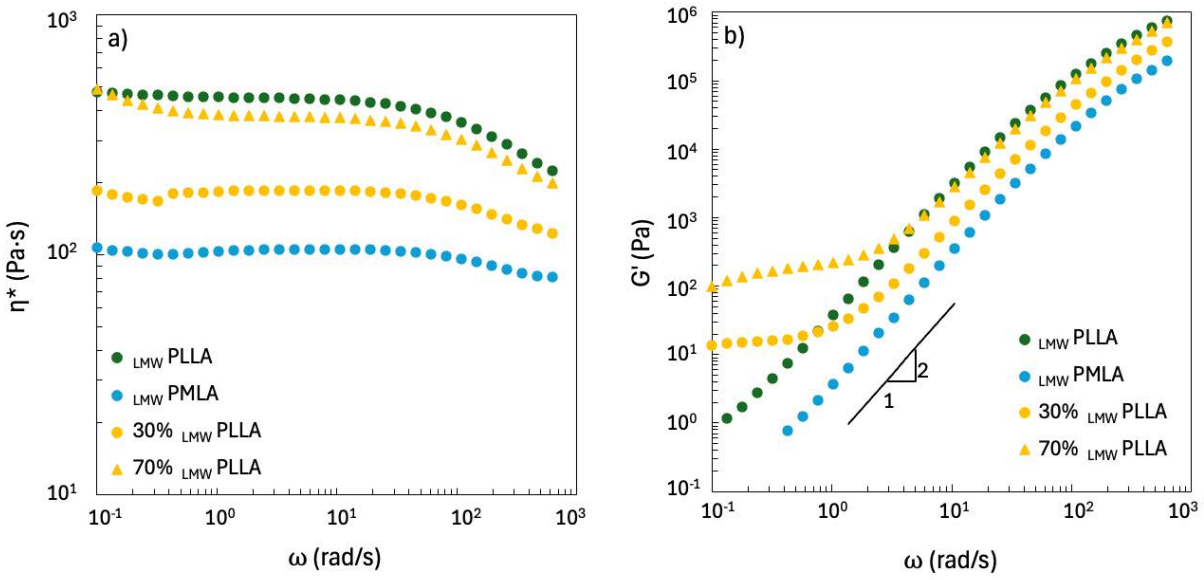

Figure 5.4 SAOS data for LMW PLLA and LMW PMLA blends obtained at 190 °C

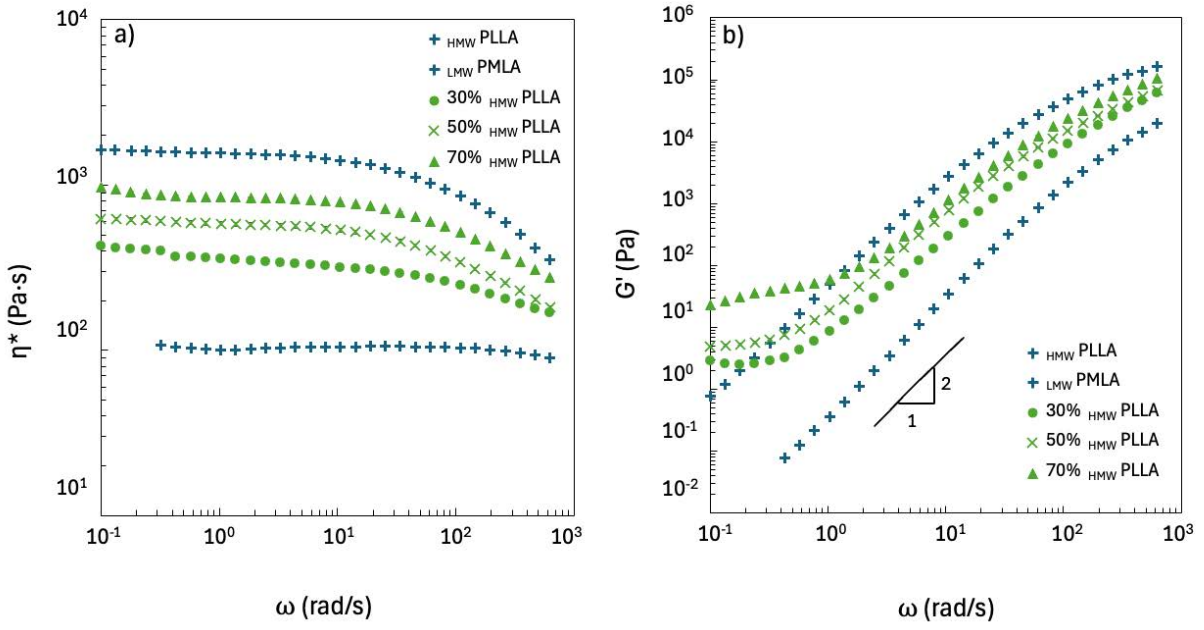

Figure 5.5 SAOS data for HMW PLLA and LMW PMLA blends obtained at 190 °C

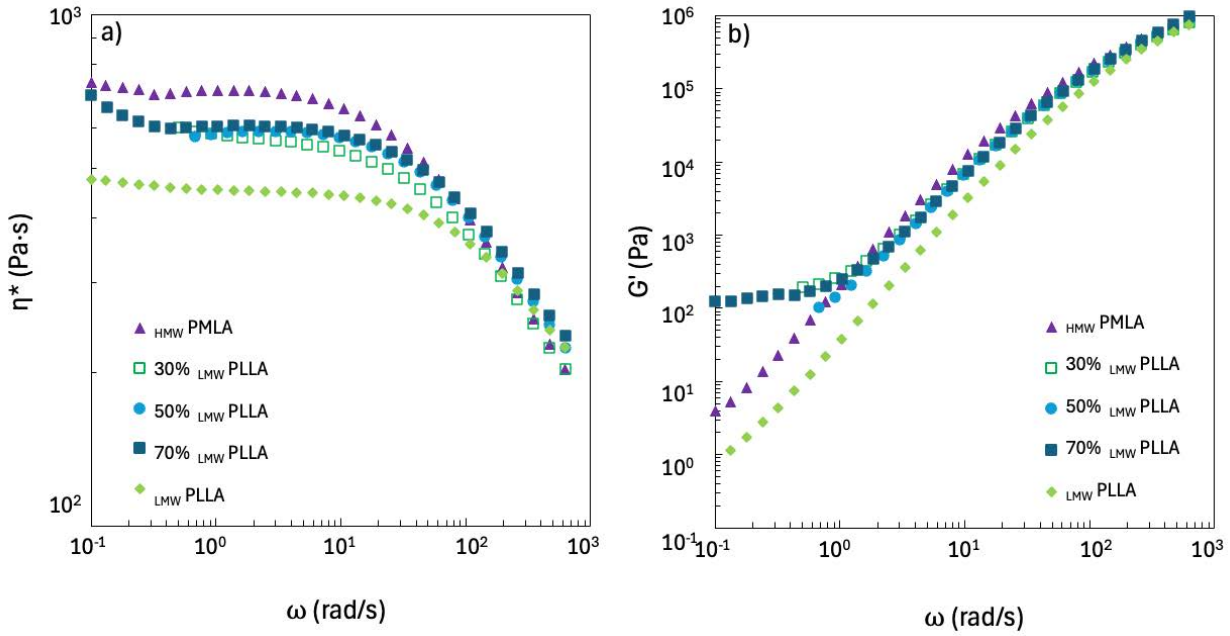

Figure 5.6 SAOS data for $_{LMW}$ PLLA and $_{HMW}$ PMLA blends obtained at 190 °C

5.2.3 Model Fitting

The Palierne model, presented in Equation 5.2, is a classic and well-known model to fit viscoelastic material with an emulsion type morphology. This model was selected because it is commonly applied to immiscible PLA-based blends with droplet–matrix morphologies. However, this model has important limitations as it assumes no interactions between phases [6].

$$G_B^*(\omega) = \frac{1 + 3\sum_i \phi_i H_i^*(\omega)}{1 - 2\sum_i \phi_i H_i^*(\omega)} G_M^*(\omega) \tag{5.2}$$

where

$$H_i^*(\omega) = \frac{4\left(\frac{\alpha}{R_v}\right)[2G_m^*(\omega) + 5G_d^*(\omega)] + [G_d^*(\omega) - G_m^*(\omega)][16G_m^*(\omega) + 19G_d^*(\omega)]}{40\left(\frac{\alpha}{R_v}\right)[G_m^*(\omega) + G_d^*(\omega)] + [2G_d^*(\omega) + 3G_m^*(\omega)][16G_m^*(\omega) + 19G_d^*(\omega)]} \tag{5.3}$$

The Gramespacher–Meissner (GM) model was also evaluated. The GM model loss and storage moduli are described by Equations 5.4 and 5.5. The relaxation time of the dispersed phase can directly be estimated from Equation 5.7. The GM model is typically considered when the Palierne model fails to adequately describe the experimental data [80]. The GM model considers slips at the interphase, unlike the Palierne model which assumes perfect stress transfer and no slip. This can arise in immiscible polymer blends with weak interfacial interactions or in the absence of compatibilization [6], [70], [80], [81]. Figure 5.7 shows the Palierne and the GM models for the blend of 10% $_{HMW}$PLLA and 90% $_{HMW}$PMLA while Tables 5.5 and 5.6 presents respectively the interfacial tension and the relaxation time of the dispersed phase obtained from both models. The GM model provided a comparable fit and yielded similar interfacial tension values to those obtained with the Palierne model. However, the relaxation time predicted by the GM model showed poorer agreement to the SAOS data than Palierne. The GM model was therefore not further pursued, as no new information was provided from this model fitting.

$$G'_{blend} = \phi_d G'_d(\omega) + (1-\phi_d)G'_m(\omega) + \frac{\eta}{\lambda_1}\left(1-\frac{\lambda_2}{\lambda_1}\right)\frac{\omega^2\lambda_1^2}{1+\omega^2\lambda_1^2} \tag{5.4}$$

$$G''_{blend} = \phi_d G''_d(\omega) + (1-\phi_d)G''_m(\omega) + \frac{\eta}{\lambda_1}\left(1-\frac{\lambda_2}{\lambda_1}\right)\frac{\omega^2\lambda_1^2}{1+\omega^2\lambda_1^2} \tag{5.5}$$

with

$$\eta = 1 + \frac{(5k+2)}{2(k+1)}\phi_d + \frac{5(5k+2)^2}{8(k+1)^2}\phi_d^2 \tag{5.6}$$

$$\lambda_1 = \lambda_0\left[1 + \frac{5(19k+16)}{4(k+1)(2k+3)}\phi_d\right] \tag{5.7}$$

$$\lambda_2 = \lambda_0 \left[1 + \frac{3(19k + 16)}{4(k + 1)(2k + 3)} \phi_d\right] \tag{5.8}$$

$$k = \frac{\eta_d}{\eta_m} \tag{5.9}$$

Where η_d and η_m are the viscosity of the dispersed phase and the matrix, G'_d and G'_m and are the storage module of the dispersed phase and the matrix, G''_d and G''_m are the loss moduli of the dispersed phase and the matrix, ω the angular frequency, ϕ_d the volume fraction of the dispersed phase.

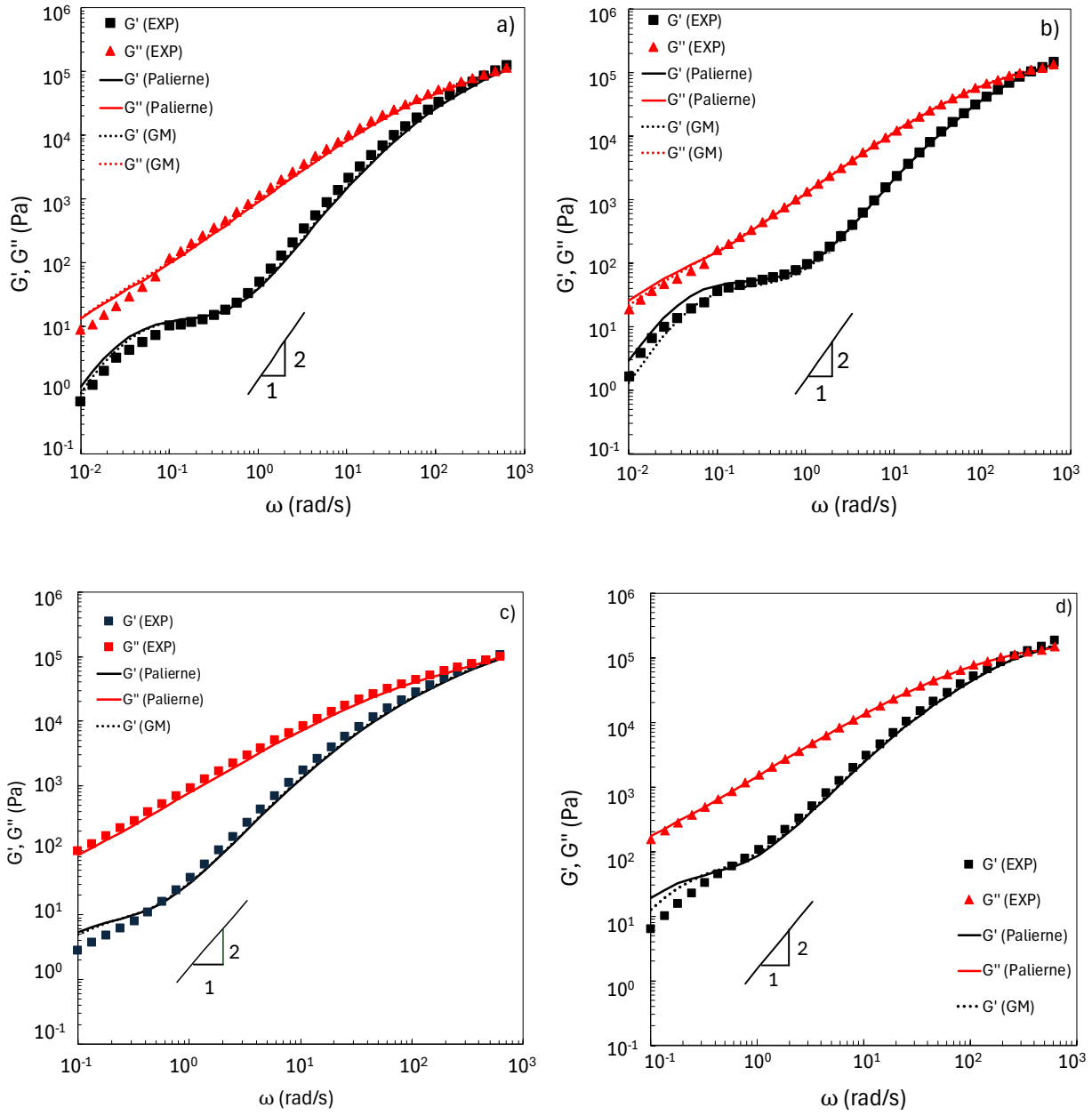

Figure 5.7 Storage and loss moduli experimental data (EXP) of (a) 30% $_{HMW}$ PLLA and (b) 70% $_{HMW}$ PMLA(c) 10% $_{HMW}$ PLLA and (d) 90% $_{HMW}$ PMLA fitted with the Palierne model and the Gramespacher–Meissner (GM) model

Table 5.5 Interfacial tension obtained from the Palierne an GM fit of the 30% and 70% $_{HMW}$ PLLA blend

$_{HMW}$ PLLA Content (%)	Radius *Rv* (μm)	Interfacial Tension α Palierne (mN/m)	Interfacial Tension α GM (mN/m)
30	1.70 ± 0.20	0.17 ± 0.02	0.73
70	0.64 ± 0.03	0.10 ± 0.01	0.50

Table 5.6 Relaxation times of the dispersed phase λ_d obtained from the relaxation spectra, from the Palierne and the GM model for 30% and 70% $_{HMW}$ PLLA blend

$_{HMW}$ PLLA Content (%)	Relaxation Time λ_d (s) from SAOS data	Relaxation Time λ_d (s) Estimated by the Palierne model	Relaxation Time λ_d (s) Estimated by the GM model
30	31	30	28
70	23	23	18

The Lee–Park model could represent a relevant alternative for future work, as it accounts for interfacial interactions. However, it is more complex to implement and was therefore beyond the scope of the present study.

5.3 Thermal Degradation

Thermal degradation was first investigated through rheology. Time sweeps were performed at 190°C during at least 30 minutes for all neat PLA and for all blends prior to SAOS measurements for new blends. As previously presented in Figure 5.3, PMLA degrades faster than PLLA.

Time sweeps where also performed on all four neat PLA pellets. Solid metal inserts mounted on the parallel-plate geometry of the MCR 302 rheometer were used for these measurements. These inserts allowed for direct comparison between pellets and compression-molded disks by melting polymer pellets directly in the rheometer prior to measurements. By avoiding the thermal pressing step required for disk preparation, this procedure minimized the thermal history and reduced the risk of degradation. Figure 5.8 compares the complex viscosity of $_{HMW}$ PLLA obtain directly from pellets with that measured from compression molded disks. The disks sample exhibit clear signs of thermal degradation due to the processing steps. This is evidenced by the lower viscosity over the entirety of the experiment and by a steeper decrease in viscosity after approximately 10 min, suggesting a more pronounced degradation than pellets samples. However, for all SAOS measurements presented in the article, the neat polymers were blended and compression-molded into disks using a thermal press to ensured consistent sample preparation and direct comparison with the blends, which were also prepared as molded disks.

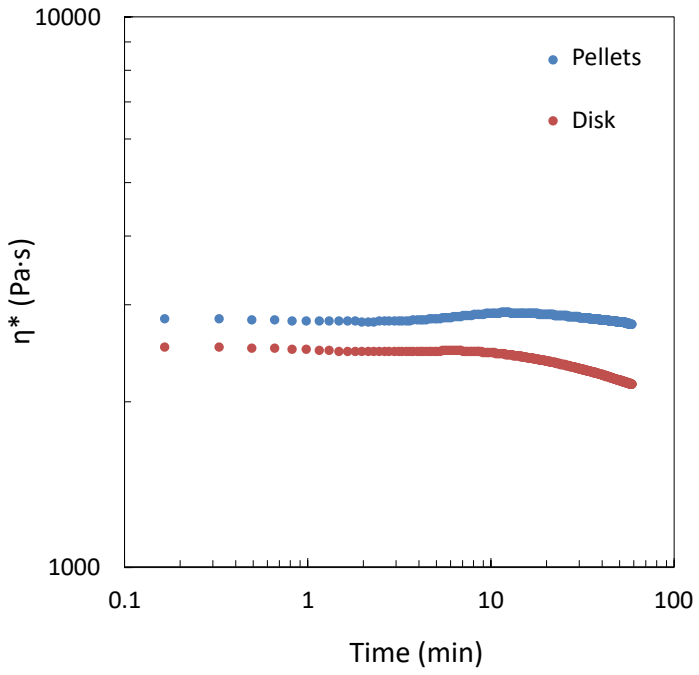

Figure 5.8 Complex viscosity of $_{HMW}$ PLLA obtain from pellets and from compression molded disks

Thermogravimetric analysis (TGA) was performed on the neat PMLA grades to evaluate their thermal stability. The results confirmed that the $_{LMW}$ PMLA exhibits thermal degradation at a lower temperature than the $_{HMW}$ PMLA, as can be seen in Figures 5.9 and 5.10. The degradation initiated in the range of 250–270 °C, which is slightly above the rheological testing temperature of 190 °C.

These results all suggests that prolonged thermal exposure influences the rheological results of PLA and contributes to variations in the measured data.

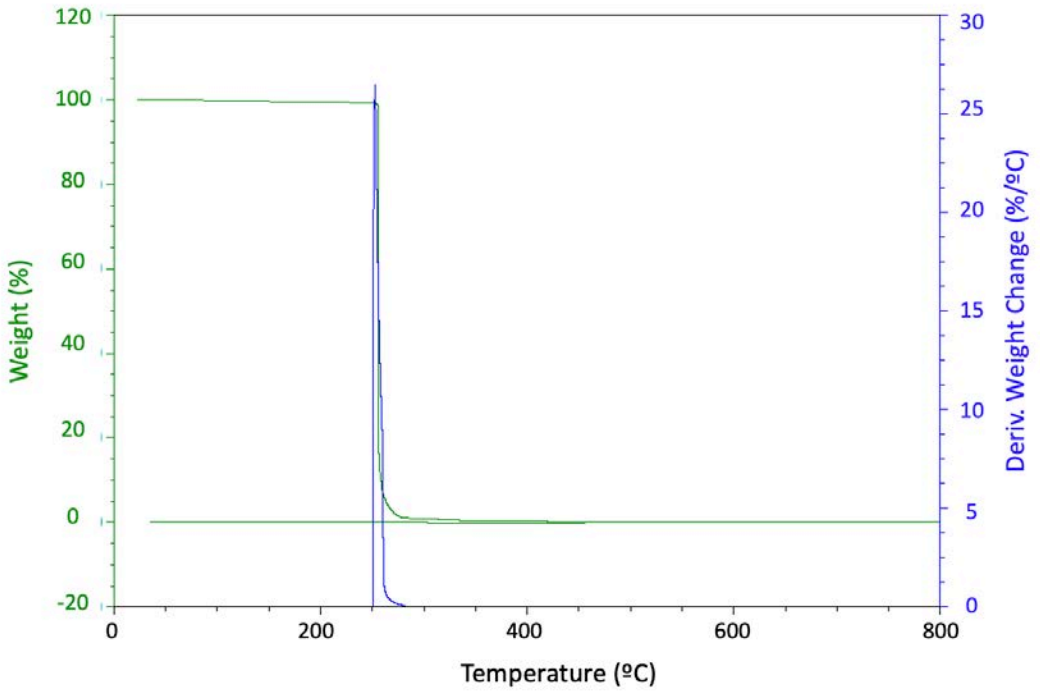

Figure 5.9 TGA results of $_{LMW}$ PMLA

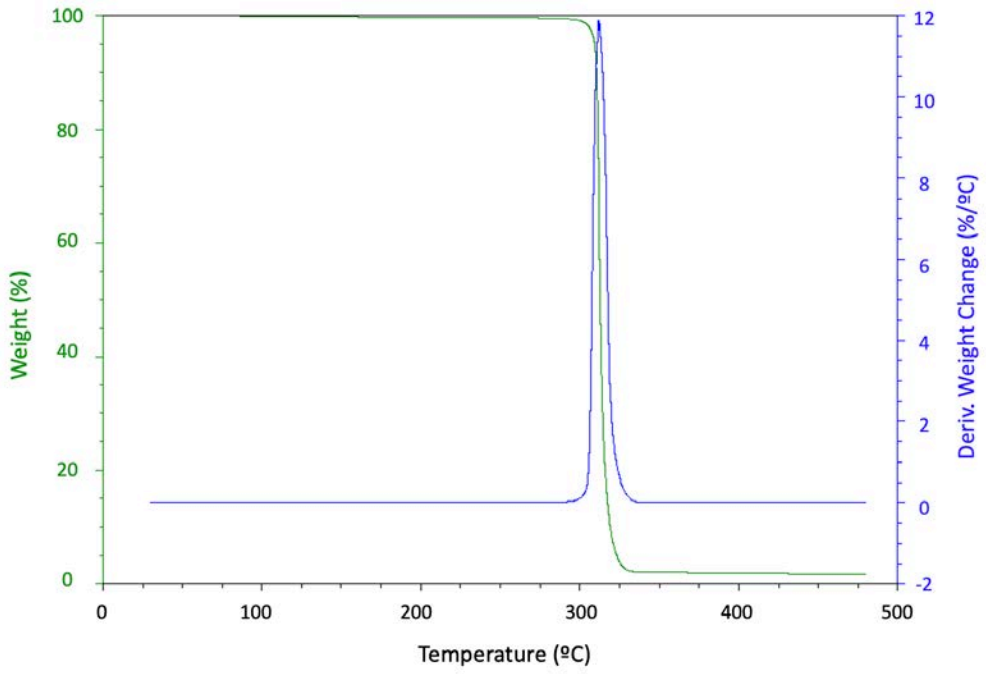

Figure 5.10 TGA results of $_{HMW}$ PMLA

5.4 Film Casting

Miscibility can be assessed by simple optical observation. For polymer blends, visual inspection of compression-molded films provides a qualitative indication of phase behavior: transparent films generally suggest miscibility due to the absence of large-scale phase separation, whereas turbidity or opacity indicates light scattering caused by phase domains, which is characteristic of immiscible systems [82].

Film casting was investing for both high molecular weight PLLA and PMLA, as well as their 70 and 90 wt% PLLA blends. Prior to film preparation, the polymers were melt-blended at 190 °C under a nitrogen atmosphere for 15 min at 50 rpm. Polymers were than molded into films of a thickness of about 200 μm by compression molding under nitrogen at 190 °C. Films were subsequently placed between room temperature metal plates in order to quench the samples. The

same conditions and equipment were used as any sample preparation done in this research to ensure comparable results.

However, as shown in Figure 5.11, the results obtain were inconclusive. The text placed behind the films remained clearly visible in all four samples, two blends and two neat polymers, indicating that no significant turbidity was observed. Turbidity would be expected in both blends, mostly in 70% (image c)) from rheological, thermal and morphology conclusions. Neat PLLA (image a) exhibits the most turbid sample, likely due to crystallization resulting from insufficient quenching during processing. Therefore, optical observations were deemed inconclusive and insufficient to draw definitive conclusions regarding the miscibility of the blends.

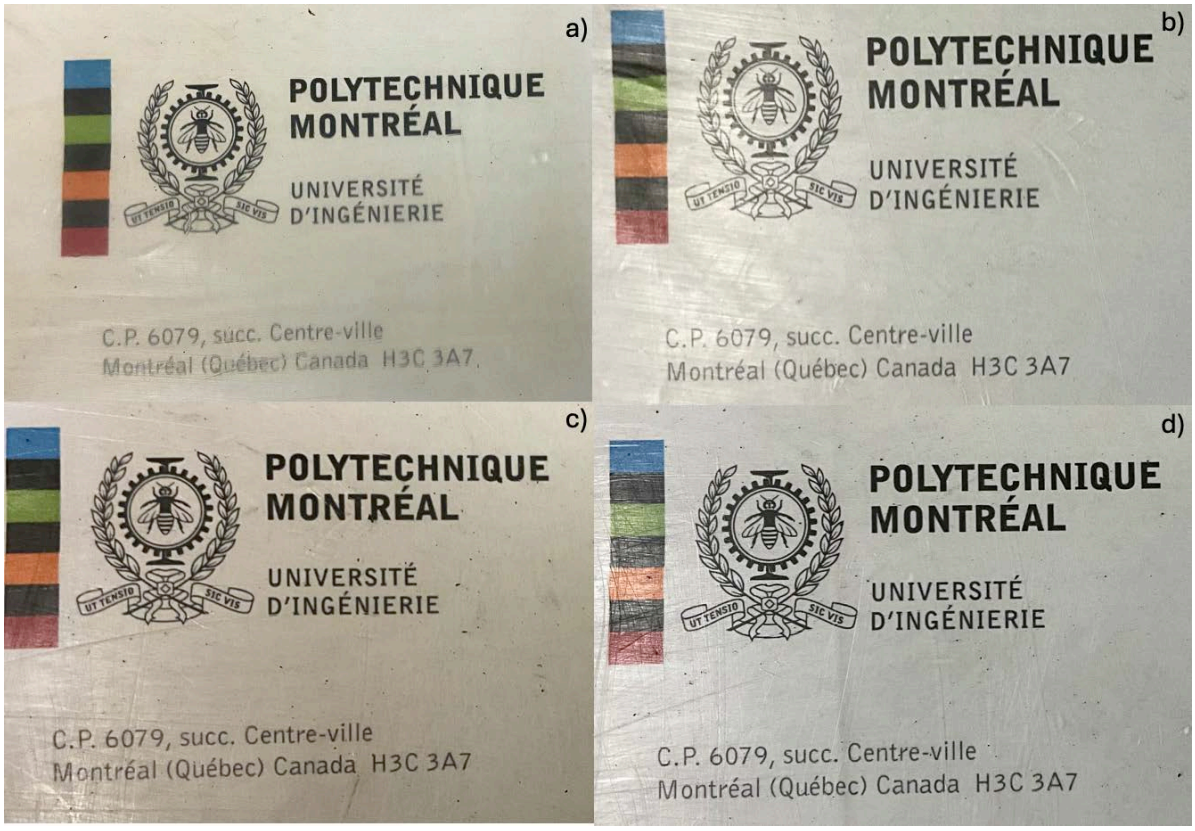

Figure 5.11 Films of thickness of around 200 μm of (a) $_{HMW}$ PLLA (b) $_{HMW}$ PMLA (c) 70/30 $_{HMW}$ PLLA/ $_{HMW}$ PMLA (d) 90/10 $_{HMW}$ PLLA/ $_{HMW}$ PMLA

5.5 Biodegradation and degradation

Biodegradation and degradation study between PMLA and PLLA were considered. Because of the structural and thermal differences between PMLA and PLLA, such as a lower glass transition temperature, it is reasonable to hypothesize that PMLA may degrade faster than PLLA. However, these investigations were abandoned due to the complexity of experimental conditions. Multiple environments and standards were considered for testing, including saline water, freshwater and compost., standardized biodegradation and degradation testing requires controlled environmental conditions and often specific factors such as elevated temperature, specific microorganisms or enzyme to trigger the degradation mechanisms. Implementing such protocols would have required additional equipment and long-term monitoring beyond the scope of this work.

Nevertheless, these analyses remain an important direction for future work. The impact of added PMLA to PLLA on degradation should be investigated as well. A systematic study would help determine whether PMLA indeed degrades more readily than PLLA and provide deeper insight on the mechanisms governing their environmental degradation.

CHAPTER 6 CONCLUSION AND RECOMMENDATIONS

This thesis aimed to clarify the behavior of poly(meso)lactide (PMLA) via blends with poly-l-lactide (PLLA). While PLLA is widely studied and industrially relevant, PMLA remains mainly uncharacterized, particularly regarding its miscibility, rheological and thermal behavior when blended with semicrystalline PLA.

The results demonstrate that PLLA/PMLA blends exhibit immiscibility and possible sign of partial miscibility at intermediate compositions, while they exhibited partial miscibility at extreme compositions. Morphological observations realized via AFM confirmed the presence of distinct phases for all blend, precisely of co-continuous morphology for the blend of 50% $_{HMW}$ PLLA and of an emulsion-type morphology for all other blends tested. They also highlighted the presence of minor phase inclusions in the major phase and vice versa for the 30% and 70% $_{HMW}$ PLLA blends.

Thermal and rheological analyses provided insight into phase behavior and miscibility as well. DSC indicated immiscibility by showcasing two different T_g for the blends of 30%, 50% and 70% $_{HMW}$ PLLA blends, but could only revealed the presence of a single T_g for the 10% and 90% $_{HMW}$ PLLA blends. SAOS measurements revealed the presence of a shoulder in the storage modulus at low frequency, indicative of interfacial tension effects. The immiscibility conclusion for the blends of 30%, 50% and 70% $_{HMW}$ PLLA blends was further supported by the presence of a relaxation mechanism associated with interfacial tension in the relaxation spectra, as well as by model fitting consistent with immiscible polymer blends, the Palierne model. The blends with suspected partial miscibility, 10% and 90% $_{HMW}$ PLLA blends, displayed a smaller relaxation mechanism associated with interfacial tension and could not be successfully fitted by either Palierne model or the ideal mixing law.

Thermal stability was also investigated, revealing that PMLA exhibits different degradation behavior compared to PLLA. A decreased in the molecular weight of PMLA also implied a lower

degradation temperature. These differences suggest that incorporation of PMLA may influence processing stability, which is critical for melt-based manufacturing techniques.

Some experimental approaches initially planned in this work could not be fully realized. Dynamic mechanical analysis (DMA) was abandoned due to demolding issues associated with the brittleness of PLA-based materials, which prevented the preparation of geometrically precise specimens required for solid-state measurements. Similarly, the intended biodegradation study was not completed, primarily due to experimental complexity and time limits. Although these aspects were not experimentally finalized, they revealed important processing limitations and highlighted the inherent brittleness of PLLA and PMLA, as well as the need for further research.

In conclusion, this thesis advances the understanding of PLLA/PMLA blends by elucidating their miscibility limits, morphological development, rheological and thermal behavior. It highlights both the potential and the limitations of incorporating PMLA into PLA-based materials, as well as clarifying rheological and thermal behavior of PMLA.

Future research should further investigate compatibilization strategies, detailed degradation mechanisms in various environments (hydrolytic, enzymatic, and composting conditions), and the influence of molecular weight on phase morphology. DMA analysis could also be pursued in order to confirm DSC findings, which were limited in the present study by instrument resolution. A deeper understanding of interfacial properties and long-term stability would also be valuable for evaluating the industrial viability of these blends.

REFERENCES

[1] Y. J. Sohn *et al.*, "Recent Advances in Sustainable Plastic Upcycling and Biopolymers," *Biotechnol. J.*, vol. 15, no. 6, p. 1900489, 2020, doi: 10.1002/biot.201900489.

[2] R. A. Auras, L.-T. Lim, S. E. M. Selke, and H. Tsuji, *Poly(lactic acid): Synthesis, Structures, Properties, Processing, Applications, and End of Life*. John Wiley & Sons, 2022.

[3] F. A. Morrison, *Understanding Rheology*. Oxford University Press, 2001.

[4] P. J. Carreau, D. C. R. D. Kee, and R. P. Chhabra, *Rheology of Polymeric Systems: Principles and Applications*. Hanser, 2021. doi: 10.1016/C2018-0-01790-9.

[5] C. W. Macosko, *Rheology: Principles, Measurements, and Applications*. Wiley, 1994.

[6] J. F. Palierne, "Linear rheology of viscoelastic emulsions with interfacial tension," *Rheol. Acta*, vol. 29, no. 3, pp. 204–214, May 1990, doi: 10.1007/BF01331356.

[7] K. Venkatramanan and V. Arumugam, "Viscosity Studies on Polypropylene Glycol and Its Blend," *Int. J. Thermophys.*, vol. 27, no. 1, pp. 66–78, Jan. 2006, doi: 10.1007/s10765-006-0021-x.

[8] H. Qiao, A. Maazouz, and K. Lamnawar, "Study of Morphology, Rheology, and Dynamic Properties toward Unveiling the Partial Miscibility in Poly(lactic acid)—Poly(hydroxybutyrate-co-hydroxyvalerate) Blends," *Polymers*, vol. 14, no. 24, Dec. 2022, doi: 10.3390/polym14245359.

[9] H. Jang, J. Lee, M. Kwon, K. Seo, and kwang soo Cho, "Analysis of PLA Blends Using Weighted Relaxation Spectrum," *Fibers Polym.*, vol. 22, Jan. 2021, doi: 10.1007/s12221-021-0121-z.

[10] J. D. Ferry, *Viscoelastic Properties of Polymers*. Wiley, 1970.

[11] M. R. Kamal, L. A. Utracki, and A. Mirzadeh, "Rheology of Polymer Alloys and Blends," in *Polymer Blends Handbook*, L. A. Utracki and C. A. Wilkie, Eds., Dordrecht: Springer Netherlands, 2014, pp. 725–873. doi: 10.1007/978-94-007-6064-6_9.

[12] N. I. N. Haris *et al.*, "A review on lactic acid production via microbial fermentation from biowaste: insights on scaling up to industrial process," *Biofuels Bioprod. Biorefining*, vol. 19, no. 2, pp. 437–452, 2025, doi: 10.1002/bbb.2704.

[13] M. A. Abdel-Rahman, Y. Tashiro, and K. Sonomoto, "Recent advances in lactic acid production by microbial fermentation processes," *Biotechnol. Adv.*, vol. 31, no. 6, pp. 877–902, Nov. 2013, doi: 10.1016/j.biotechadv.2013.04.002.

[14] B. L. C. Cunha *et al.*, "Lactide: Production Routes, Properties, and Applications," *Bioengineering*, vol. 9, no. 4, p. 164, Apr. 2022, doi: 10.3390/bioengineering9040164.

[15] A. Södergård, M. Stolt, and S. Inkinen, "Industrial Production of High-Molecular-Weight Poly(lactic Acid)," in *Poly(Lactic Acid)*, John Wiley & Sons, Ltd, 2022, pp. 29–44. doi: 10.1002/9781119767480.ch3.

[16] C. Moya-Lopez *et al.*, "Polylactide Perspectives in Biomedicine: From Novel Synthesis to the Application Performance," *Pharmaceutics*, vol. 14, no. 8, p. 1673, Aug. 2022, doi: 10.3390/pharmaceutics14081673.

[17] J. Randall *et al.*, "Comparing the Structural, Thermal, and Rheological Properties of Poly(meso-lactide) to Poly(l-lactide) and Poly(rac-lactide)," *Macromolecules*, vol. 57, no. 6, pp. 2715–2728, Mar. 2024, doi: 10.1021/acs.macromol.3c02029.

[18] M. J. Stanford and A. P. Dove, "Stereocontrolled ring-opening polymerisation of lactide," *Chem. Soc. Rev.*, vol. 39, no. 2, pp. 486–494, Jan. 2010, doi: 10.1039/B815104K.

[19] J. R. Dorgan, "Rheology of Poly(lactic Acid)," in *Poly(Lactic Acid)*, John Wiley & Sons, Ltd, 2022, pp. 153–167. doi: 10.1002/9781119767480.ch9.

[20] D. Henton, P. Gruber, J. Lunt, and J. Randall, "Polylactic Acid Technology," in *Natural Fibers, Biopolymers, and Biocomposites*, 2005. doi: 10.1201/9780203508206.ch16.

[21] L. Fambri and C. Migliaresi, "Crystallization and Thermal Properties," in *Poly(Lactic Acid)*, John Wiley & Sons, Ltd, 2022, pp. 135–151. doi: 10.1002/9781119767480.ch8.

[22] L. Feng, B. Zhang, X. Bian, G. Li, Z. Chen, and X. Chen, "Thermal Properties of Polylactides with Different Stereoisomers of Lactides Used as Comonomers," *Macromolecules*, vol. 50, no. 16, pp. 6064–6073, Aug. 2017, doi: 10.1021/acs.macromol.7b00818.

[23] J. Dorgan, J. Janzen, M. Clayton, S. Hait, and D. Knauss, "Melt rheology of variable L-content poly(lactic acid)," *J. Rheol. - J RHEOL*, vol. 49, May 2005, doi: 10.1122/1.1896957.

[24] P. Pan, W. Kai, B. Zhu, T. Dong, and Y. Inoue, "Polymorphous Crystallization and Multiple Melting Behavior of Poly(l-lactide): Molecular Weight Dependence," *Macromolecules*, vol. 40, no. 19, pp. 6898–6905, Sep. 2007, doi: 10.1021/ma071258d.

[25] A. A. Cuadri and J. E. Martín-Alfonso, "Thermal, thermo-oxidative and thermomechanical degradation of PLA: A comparative study based on rheological, chemical and thermal properties," *Polym. Degrad. Stab.*, vol. 150, pp. 37–45, Apr. 2018, doi: 10.1016/j.polymdegradstab.2018.02.011.

[26] V. Taubner and R. Shishoo, "Influence of processing parameters on the degradation of poly(L-lactide) during extrusion," *J. Appl. Polym. Sci.*, vol. 79, no. 12, pp. 2128–2135, 2001, doi: 10.1002/1097-4628(20010321)79:12<2128::AID-APP1020>3.0.CO;2-#.

[27] M. Oliveira, E. Santos, A. Araújo, G. J. M. Fechine, A. V. Machado, and G. Botelho, "The role of shear and stabilizer on PLA degradation," *Polym. Test.*, vol. 51, pp. 109–116, May 2016, doi: 10.1016/j.polymertesting.2016.03.005.

[28] I. Velghe, B. Buffel, V. Vandeginste, W. Thielemans, and F. Desplentere, "Review on the Degradation of Poly(lactic acid) during Melt Processing," *Polymers*, vol. 15, no. 9, p. 2047, Apr. 2023, doi: 10.3390/polym15092047.

[29] M. Kervran, C. Vagner, M. Cochez, M. Ponçot, M. R. Saeb, and H. Vahabi, "Thermal degradation of polylactic acid (PLA)/polyhydroxybutyrate (PHB) blends: A systematic review," *Polym. Degrad. Stab.*, vol. 201, p. 109995, Jul. 2022, doi: 10.1016/j.polymdegradstab.2022.109995.

[30] T. Yang, R. Lu, J. Yan, S. Jin, and Y. Xue, "Influence of molecular weight on the thermal degradation of poly(lactic acid): A crystallization perspective," *Polymer*, vol. 335, p. 128839, Sep. 2025, doi: 10.1016/j.polymer.2025.128839.

[31] T. Yang, S. He, P. Liu, J. Yan, R. Lu, and Y. Xue, "Chain heterogeneity of poly(lactic acid) and its influence on crystallization kinetics," *Int. J. Biol. Macromol.*, vol. 277, p. 134101, Oct.

2024, doi: 10.1016/j.ijbiomac.2024.134101.

[32] E. Castro-Aguirre, F. Iñiguez-Franco, H. Samsudin, X. Fang, and R. Auras, “Poly(lactic acid)—Mass production, processing, industrial applications, and end of life,” *Adv. Drug Deliv. Rev.*, vol. 107, pp. 333–366, Dec. 2016, doi: 10.1016/j.addr.2016.03.010.

[33] M. Nofar, G. Perego, and G. D. Cella, “Mechanical Properties,” in *Poly(Lactic Acid)*, John Wiley & Sons, Ltd, 2022, pp. 169–190. doi: 10.1002/9781119767480.ch10.

[34] J. Dorgan, J. Williams, and D. Lewis, “Melt Rheology of poly(lactic acid): Entanglement and chain architecture affects,” *J. Rheol. - J RHEOL*, vol. 43, pp. 1141–1155, Sep. 1999, doi: 10.1122/1.551041.

[35] J. R. Dorgan, “Rheology of Poly(Lactic Acid),” in *Poly(Lactic Acid)*, John Wiley & Sons, Ltd, 2010, pp. 125–139. doi: 10.1002/9780470649848.ch10.

[36] H. Yang and J. Du, “Crystallinity, Rheology, and Mechanical Properties of Low-/High-Molecular-Weight PLA Blended Systems,” *Molecules*, vol. 29, no. 1, p. 169, Dec. 2023, doi: 10.3390/molecules29010169.

[37] E. Saldivar-Guerra, E. Vivaldo-Lima, E. Saldivar-Guerra, and E. Vivaldo-Lima, *Handbook of Polymer Synthesis, Characterization, and Processing*. Newark, UNITED STATES: John Wiley & Sons, Incorporated, 2013. Accessed: Feb. 04, 2026. [Online]. Available: http://ebookcentral.proquest.com/lib/polymtl-ebooks/detail.action?docID=1117316

[38] E. Manias and L. A. Utracki, “Thermodynamics of Polymer Blends,” in *Polymer Blends Handbook*, L. A. Utracki and C. A. Wilkie, Eds., Dordrecht: Springer Netherlands, 2014, pp. 171–289. doi: 10.1007/978-94-007-6064-6_4.

[39] S. Jeong, “Investigation of intrinsic characteristics of polymer blends via molecular simulation: a review,” *Korea-Aust. Rheol. J.*, vol. 35, no. 4, pp. 249–266, Nov. 2023, doi: 10.1007/s13367-023-00076-9.

[40] K. Hamad, M. Kaseem, M. Ayyoob, J. Joo, and F. Deri, “Polylactic acid blends: The future of green, light and tough,” *Prog. Polym. Sci.*, vol. 85, pp. 83–127, Oct. 2018, doi: 10.1016/j.progpolymsci.2018.07.001.

[41] M. Nofar, D. Sacligil, P. J. Carreau, M. R. Kamal, and M.-C. Heuzey, “Poly (lactic acid) blends: Processing, properties and applications,” *Int. J. Biol. Macromol.*, vol. 125, pp. 307–360, Mar. 2019, doi: 10.1016/j.ijbiomac.2018.12.002.

[42] Y. Iguchi, K. Miyamoto, S. Akasaka, and S. Asai, “Formation of polylactide stereocomplex crystallites and the electrical properties of carbon black-filled PLLA/PDLA composites,” *Polym. J.*, vol. 52, no. 9, pp. 1093–1102, Sep. 2020, doi: 10.1038/s41428-020-0354-5.

[43] T. Okihara *et al.*, “Crystal structure of stereocomplex of poly(L-lactide) and poly(D-lactide),” *J. Macromol. Sci. Part B*, vol. 30, no. 1–2, pp. 119–140, Mar. 1991, doi: 10.1080/00222349108245788.

[44] Y. Li *et al.*, “Stereocomplex crystallite network in poly(D,L-lactide): formation, structure and the effect on shape memory behaviors and enzymatic hydrolysis of poly(D,L-lactide),” *RSC Adv.*, vol. 5, no. 31, pp. 24352–24362, Mar. 2015, doi: 10.1039/C5RA01624J.

[45] P. Pan, Z. Liang, B. Zhu, T. Dong, and Y. Inoue, “Blending Effects on Polymorphic Crystallization of Poly(l-lactide),” *Macromolecules*, vol. 42, no. 9, pp. 3374–3380, May 2009, doi:

10.1021/ma8024943.

[46] H. Tsuji and Y. Ikada, “Blends of isotactic and atactic poly(lactide)s: 2. Molecular-weight effects of atactic component on crystallization and morphology of equimolar blends from the melt,” *Polymer*, vol. 37, no. 4, pp. 595–602, Jan. 1996, doi: 10.1016/0032-3861(96)83146-6.

[47] L. Bouapao, H. Tsuji, K. Tashiro, J. Zhang, and M. Hanesaka, “Crystallization, spherulite growth, and structure of blends of crystalline and amorphous poly(lactide)s,” *Polymer*, vol. 50, no. 16, pp. 4007–4017, Jul. 2009, doi: 10.1016/j.polymer.2009.06.040.

[48] C.-C. Chen, J.-Y. Chueh, H. Tseng, H.-M. Huang, and S.-Y. Lee, “Preparation and characterization of biodegradable PLA polymeric blends,” *Biomaterials*, vol. 24, no. 7, pp. 1167–1173, Mar. 2003, doi: 10.1016/S0142-9612(02)00466-0.

[49] W. Groot, J. van Krieken, O. Sliekersl, and S. de Vos, “Production and Purification of Lactic Acid and Lactide,” in *Poly(Lactic Acid)*, John Wiley & Sons, Ltd, 2022, pp. 1–18. doi: 10.1002/9781119767480.ch1.

[50] K. S. Anderson, K. M. Schreck, and M. A. Hillmyer, “Toughening Polylactide,” *Polym. Rev.*, vol. 48, no. 1, pp. 85–108, Feb. 2008, doi: 10.1080/15583720701834216.

[51] R. Pantani and A. Sorrentino, “Influence of crystallinity on the biodegradation rate of injection-moulded poly(lactic acid) samples in controlled composting conditions,” *Polym. Degrad. Stab.*, vol. 98, no. 5, pp. 1089–1096, May 2013, doi: 10.1016/j.polymdegradstab.2013.01.005.

[52] S. Shrestha, M. Snowdon, and D. B. Levin, “Enzymatic Degradation of PLA: Preferential Degradation of the Amorphous Fraction,” *Polymers*, vol. 17, no. 22, Nov. 2025, doi: 10.3390/polym17223042.

[53] S. Dufour *et al.*, “A comprehensive mechanism of polyester enzymatic depolymerization: A novel singular key parameter for streamlined eco-design,” *J. Hazard. Mater.*, vol. 494, p. 138544, Aug. 2025, doi: 10.1016/j.jhazmat.2025.138544.

[54] S. Zhang, Y. Weng, and C. Ma, “Quantitative Nanomechanical Mapping of Polyolefin Elastomer at Nanoscale with Atomic Force Microscopy,” *Nanoscale Res. Lett.*, vol. 16, no. 1, p. 113, Jul. 2021, doi: 10.1186/s11671-021-03568-1.

[55] Y. He, Y. Yan, and Y. Geng, “Morphology measurements by AFM tapping without causing surface damage: A phase shift characterization,” *Ultramicroscopy*, vol. 254, p. 113832, Dec. 2023, doi: 10.1016/j.ultramic.2023.113832.

[56] J. Mathurin, A. Deniset-Besseau, D. Bazin, E. Dartois, M. Wagner, and A. Dazzi, “Photothermal AFM-IR spectroscopy and imaging: Status, challenges, and trends,” *J. Appl. Phys.*, vol. 131, no. 1, p. 010901, Jan. 2022, doi: 10.1063/5.0063902.

[57] M. Nofar, M. C. Heuzey, P. J. Carreau, M. R. Kamal, and J. Randall, “Coalescence in PLA-PBAT blends under shear flow: Effects of blend preparation and PLA molecular weight,” *J. Rheol.*, vol. 60, no. 4, pp. 637–648, Jul. 2016, doi: 10.1122/1.4953446.

[58] S. A. Saltikov, “The Determination of the Size Distribution of Particles in an Opaque Material from a Measurement of the Size Distribution of Their Sections,” in *Stereology*, H. Elias, Ed., Berlin, Heidelberg: Springer, 1967, pp. 163–173. doi: 10.1007/978-3-642-88260-9_31.

[59] J. Weese, “A regularization method for nonlinear ill-posed problems,” *Comput. Phys. Commun.*, vol. 77, no. 3, pp. 429–440, Nov. 1993, doi: 10.1016/0010-4655(93)90187-H.

[60] X. Liang, “Visualization of Nanomechanical Properties of Polymer Composites Using Atomic Force Microscopy,” *Polym. J.*, vol. 55, no. 9, pp. 913–920, Sep. 2023, doi: 10.1038/s41428-023-00790-9.

[61] A. Bahrami, C. Bailly, and B. Nysten, “Spatial resolution and property contrast in local mechanical mapping of polymer blends using AFM dynamic force spectroscopy,” *Polymer*, vol. 165, pp. 180–190, Feb. 2019, doi: 10.1016/j.polymer.2019.01.023.

[62] B. D. Favis, “Morphology development of polymer blends,” in *Polymer Blends*, vol. 1, 2 vols., C. B. Bucknall and D. R. Paul, Eds., New York: John Wiley & Sons, 2000.

[63] V. García-Masabet *et al.*, “PLA/PA Bio-Blends: Induced Morphology by Extrusion,” *Polymers*, vol. 12, no. 1, Dec. 2019, doi: 10.3390/polym12010010.

[64] S. Bärwinkel, A. Seidel, S. Hobeika, R. Hufen, M. Mörl, and V. Altstädt, “Morphology Formation in PC/ABS Blends during Thermal Processing and the Effect of the Viscosity Ratio of Blend Partners,” *Materials*, vol. 9, no. 8, Aug. 2016, doi: 10.3390/ma9080659.

[65] X. Lu, J. Zhao, X. Yang, and P. Xiao, “Morphology and properties of biodegradable poly (lactic acid)/poly (butylene adipate-co-terephthalate) blends with different viscosity ratio,” *Polym. Test.*, vol. 60, pp. 58–67, Jul. 2017, doi: 10.1016/j.polymertesting.2017.03.008.

[66] E. Meaurio, N. López-Rodríguez, and J. R. Sarasua, “Infrared Spectrum of Poly(l-lactide): Application to Crystallinity Studies,” *Macromolecules*, vol. 39, no. 26, pp. 9291–9301, Dec. 2006, doi: 10.1021/ma061890r.

[67] E. Meaurio, E. Zuza, N. López-Rodríguez, and J. R. Sarasua, “Conformational Behavior of Poly(l-lactide) Studied by Infrared Spectroscopy,” *J. Phys. Chem. B*, vol. 110, no. 11, pp. 5790–5800, Mar. 2006, doi: 10.1021/jp055203u.

[68] J. H. Kim, B. R. Min, and Y. S. Kang, “Thermodynamic Model of the Glass Transition Behavior for Miscible Polymer Blends,” *Macromolecules*, vol. 39, no. 3, pp. 1297–1299, Feb. 2006, doi: 10.1021/ma052436a.

[69] I. M. Kalogeras and W. Brostow, “Glass transition temperatures in binary polymer blends,” *J. Polym. Sci. Part B Polym. Phys.*, vol. 47, no. 1, pp. 80–95, 2009, doi: 10.1002/polb.21616.

[70] M. Elhamnia, G. H. Motlagh, and S. H. Jafari, “A multiple approach in determination of interfacial tension of biodegradable melt-mixed PBAT/EVOH blends: Correlation of morphology, rheology and mechanical properties,” *Polym. Test.*, vol. 82, p. 106301, Feb. 2020, doi: 10.1016/j.polymertesting.2019.106301.

[71] M. Nofar, A. Maani, H. Sojoudi, M. C. Heuzey, and P. J. Carreau, “Interfacial and rheological properties of PLA/PBAT and PLA/PBSA blends and their morphological stability under shear flow,” *J. Rheol.*, vol. 59, no. 2, pp. 317–333, Mar. 2015, doi: 10.1122/1.4905714.

[72] C. Lacroix, M. Aressy, and P. J. Carreau, “Linear viscoelastic behavior of molten polymer blends: A comparative study of the Palierne and Lee and Park models,” *Rheol. Acta*, vol. 36, no. 4, pp. 416–428, Jul. 1997, doi: 10.1007/BF00396328.

[73] P. J. Carreau, M. Bousmina, and A. Ajji, “Rheological Properties of Blends: Facts and Challenges,” in *Progress in Pacific Polymer Science 3*, K. P. Ghiggino, Ed., Berlin, Heidelberg: Springer, 1994, pp. 25–39. doi: 10.1007/978-3-642-78759-1_3.

[74] V. Speranza, A. De Meo, and R. Pantani, “Thermal and hydrolytic degradation kinetics of

PLA in the molten state," *Polym. Degrad. Stab.*, vol. 100, pp. 37–41, Feb. 2014, doi: 10.1016/j.polymdegradstab.2013.12.031.

[75] Y.-M. Corre, J. Duchet, J. Reignier, and A. Maazouz, "Melt strengthening of poly (lactic acid) through reactive extrusion with epoxy-functionalized chains," *Rheol. Acta*, vol. 50, no. 7, pp. 613–629, Aug. 2011, doi: 10.1007/s00397-011-0538-1.

[76] T. Cui, S. Liu, M. H. Wagner, and Q. Huang, "Consistent modeling of nonlinear shear and elongational start-up data of entangled polystyrene solutions," *Rheol. Acta*, vol. 64, no. 6, pp. 255–261, Jul. 2025, doi: 10.1007/s00397-025-01494-y.

[77] Z. Gui, H. Wang, Y. Gao, C. Lu, and S. Cheng, "Morphology and melt rheology of biodegradable poly(lactic acid)/poly(butylene succinate adipate) blends: effect of blend compositions," *Iran. Polym. J.*, vol. 21, no. 2, pp. 81–89, Feb. 2012, doi: 10.1007/s13726-011-0009-7.

[78] R. Salehiyan, S. S. Ray, F. J. Stadler, and V. Ojijo, "Rheology–Microstructure Relationships in Melt-Processed Polylactide/Poly(vinylidene Fluoride) Blends," *Materials*, vol. 11, no. 12, Dec. 2018, doi: 10.3390/ma11122450.

[79] D. Graebling, R. Muller, and J. F. Palierne, "Linear viscoelastic behavior of some incompatible polymer blends in the melt. Interpretation of data with a model of emulsion of viscoelastic liquids," *Macromolecules*, vol. 26, no. 2, pp. 320–329, Jan. 1993, doi: 10.1021/ma00054a011.

[80] H. Gramespacher and J. Meissner, "Interfacial tension between polymer melts measured by shear oscillations of their blends," *J. Rheol.*, vol. 36, no. 6, pp. 1127–1141, Aug. 1992, doi: 10.1122/1.550304.

[81] M. K. Kwon and K. S. Cho, "Analysis of the Palierne model by relaxation time spectrum," *Korea-Aust. Rheol. J.*, vol. 28, no. 1, pp. 23–31, Feb. 2016, doi: 10.1007/s13367-016-0002-y.

[82] C. Samuel, J.-M. Raquez, and P. Dubois, "PLLA/PMMA blends: A shear-induced miscibility with tunable morphologies and properties?," *Polymer*, vol. 54, no. 15, pp. 3931–3939, Jul. 2013, doi: 10.1016/j.polymer.2013.05.021.

APPENDIX A ARTICLE SUPPLEMENTARY MATERIAL

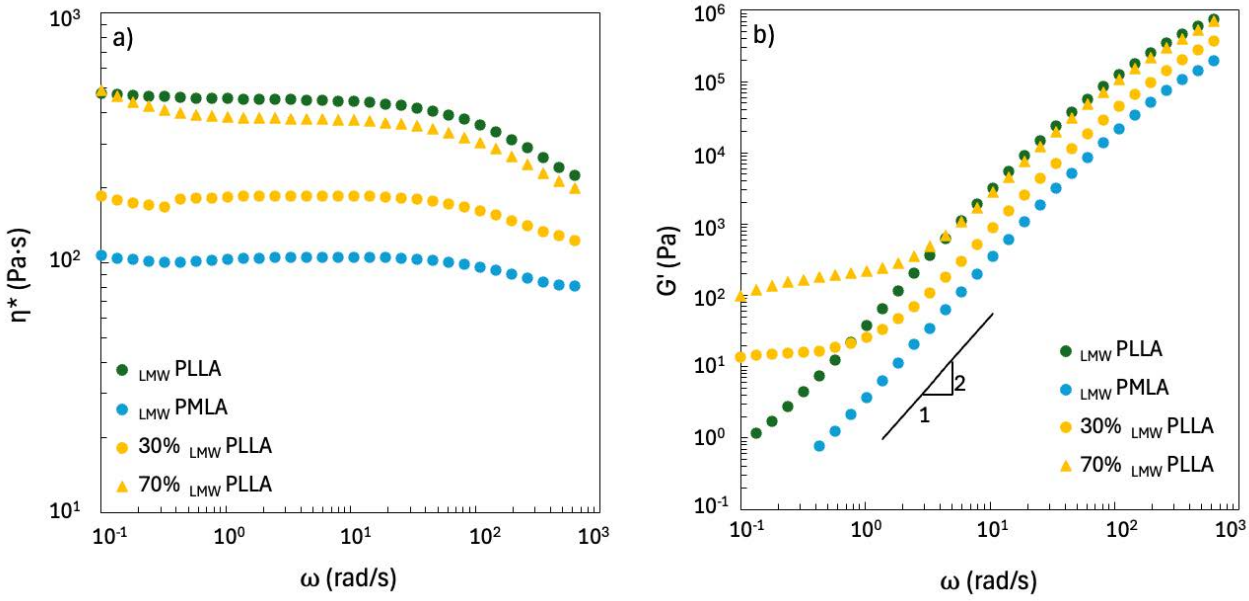

Figure S1. SAOS data for $_{LMW}$ PLLA and $_{LMW}$ PMLA blends obtained at 190 °C

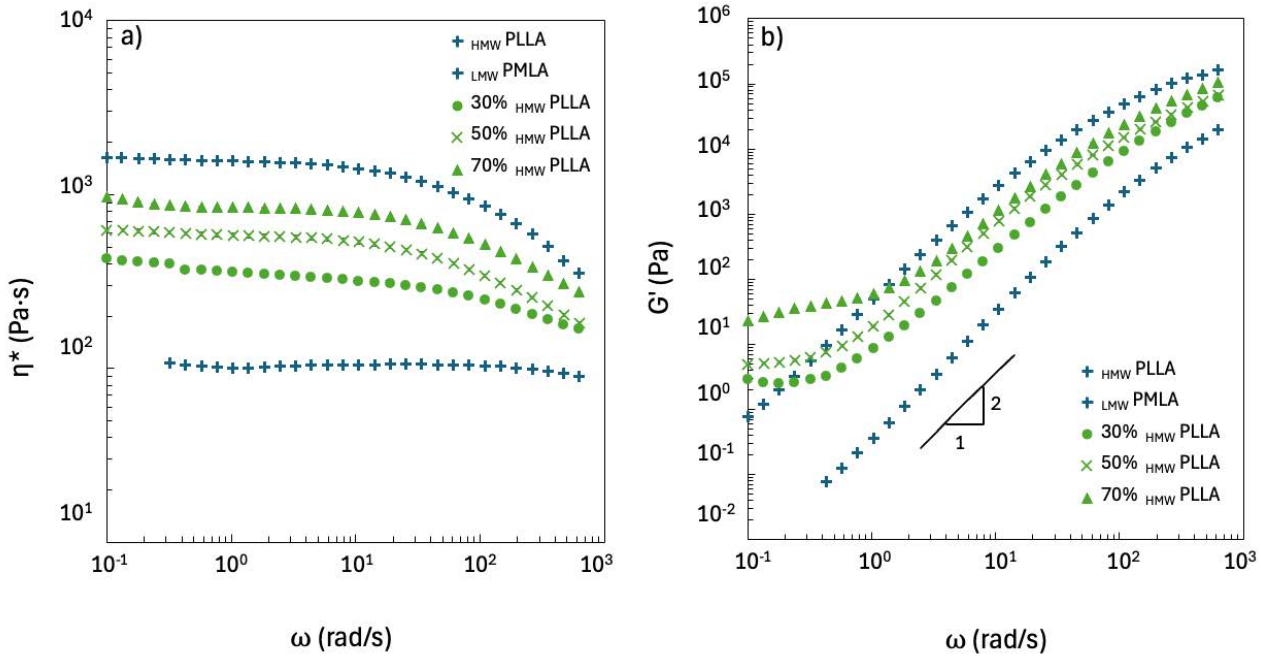

Figure S2. SAOS data for $_{HMW}$ PLLA and $_{LMW}$ PMLA blends obtained at 190 °C

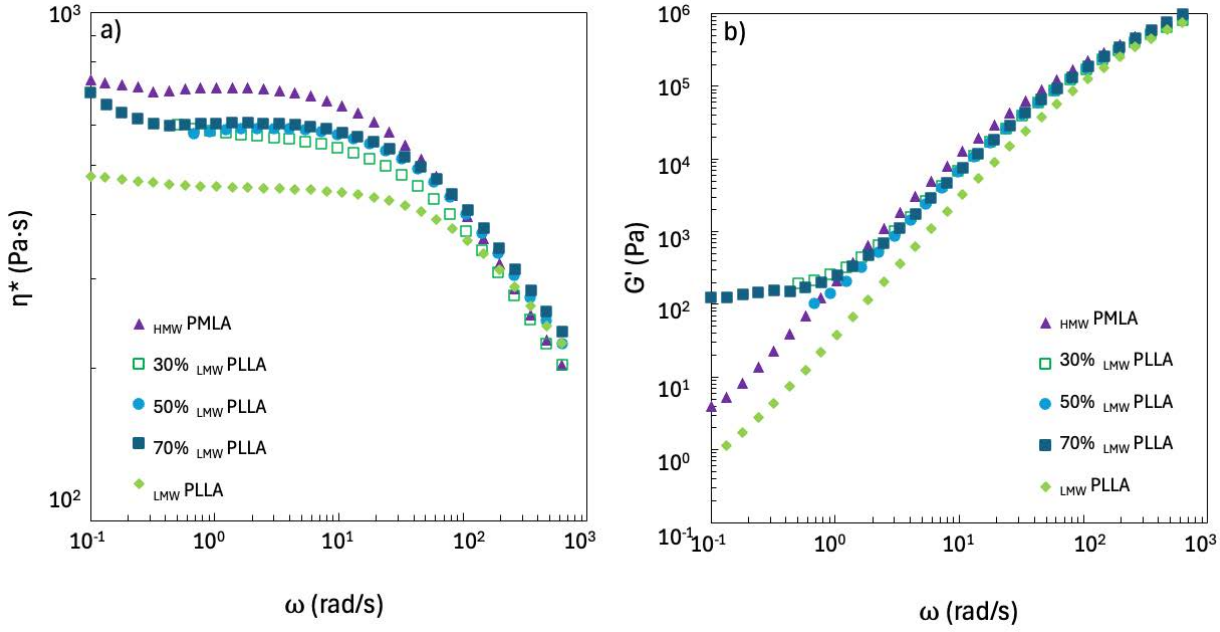

Figure S3. SAOS data for $_{LMW}$ PLLA and $_{HMW}$ PMLA blends obtained at 190 °C